WILEY | Hindawi

Research Article

Pore Structure Characteristics, Genesis, and Its Controlling Effect on Gas Migration of Quaternary Mudstone Reservoir in Qaidam Basin

Shijie He,[1,2] **Xianglu Tang** ®**,**[1,2] **Zeyu Shao,**[3] **Zhenxue Jiang,**[1,2] **Bo Wang,**[3] **Xiaoxue Liu,**[1,2] **Yuchao Wang,**[1,2] **and Mingli Xu**[1,2]

[1]*State Key Laboratory of Petroleum Resources and Prospecting, China University of Petroleum, Beijing 102249, China*
[2]*China University of Petroleum, Beijing 102249, China*
[3]*Exploration and Development Institute of Qinghai Oilfield Company, PetroChina, Dunhuang, Gansu 736202, China*

Correspondence should be addressed to Xianglu Tang; tangxl@cup.edu.cn

The Sanhu Depression in Qaidam Basin is the largest Quaternary biogenic gas exploration area with the shallowest burial depth in the world. The shallow high abundance of gas reservoirs and high-quality pure methane have become the main production areas. The development characteristics of loose mudstone reservoirs are restricted by extreme heterogeneity. Therefore, the Quaternary Qigequan Formation mudstone in Qaidam Basin is selected as the research object. Based on the study of the sedimentary background, petrological characteristics, and pore structure characteristics, by comparing the characteristics of different mudstone reservoirs, the controlling factors of the development of different mudstone reservoirs and the control of gas migration are clarified. Research shows the following: (1) The mudstone reservoirs of the Qigequan Formation mainly develop intergranular pores, clay mineral pores, and intragranular pores. The pore size distribution varies from nanometers to micrometers, and mesopores mainly contribute to the specific surface area. (2) Rigid minerals and clay minerals are the main controlling factors for the pore structure of mudstone reservoirs. The increase in the content of rigid minerals is conducive to the development of macropores or larger micropores, while the increase in the content of clay minerals is conducive to the development of mesopores and provides an important specific surface area for gas adsorption. (3) The gas migration form of pure mudstone is mainly dominated by Fick diffusion and slippage flow, which has the characteristics of self-sealing accumulation. The gas migration form of silty mudstone is the coexistence of Fick diffusion, slippage flow, and Darcy flow, which has the features of self-sealing and Darcy flow accumulation. The gas migration form of sandy mudstone is mainly Darcy flow, only with Darcy flow accumulation characteristics. The flow form of gas creates different accumulation modes of mudstone biogas. The Quaternary mudstone reservoir shows different particularity under different material components, and the exploration targets should be treated differently according to specific mudstone types.

1. Introduction

Qaidam Basin is a large Mesozoic-Cenozoic inland sedimentary basin with its attitude measuring 2650-3000 m, surrounded by the Altun Mountain in the northwest, Qilian Mountain in the northeast, and Kunlun Mountain in the southwest [1, 2]. The Qigequan Formation is the primary sedimentary strata in the eastern Qaidam Basin, with a thickness of nearly 3000 m. The Qigequan Formation pro-vides sufficient gas source rocks to form Quaternary biogas [3, 4]. Biogas resources account for approximately 20% percent of the world's natural gas resources and have significant economic value. As a large-scale biogas accumulation area of the Quaternary, the unique geological conditions of the Sebei gas field are very representative, and its successful exploration and development experience has specific reference significance [5]. Previous studies in this area used mudstone as source rock and sandstone as a conventional

reservoir. The exploration prospect of unconventional oil and gas was seriously underestimated. With the continuous advancement of exploration and development technology, primarily the breakthrough of horizontal wells and hydraulic fracturing technology, the abundant hydrocarbon resources in mudstone, which is the source rock or cap layer of conventional oil and gas reservoirs, have received widespread attention. Micro-nanopores are developed in mudstone reservoirs, and the pore structure controls the occurrence state, gas content, seepage capacity, and microhydrocarbon migration and accumulation mechanism of mudstone gas [6–8]. Therefore, the study of micro-nanopore structure characterization of mudstone is helpful to improve the prediction and characterization of the gas storage, hydrocarbon migration, and accumulation properties of mudstone reservoirs.

The experimental methods of pore structure characterization can mainly be divided into imaging, fluid, and nonfluid invasion methods [9–11]. Imaging methods mainly include field emission scanning electron microscopy (FE-SEM), focused ion beam scanning electron microscopy (FIB-SEM), and atomic force microscopy (AFM), which can observe the pore size, morphology, and distribution of samples at different scales [12–14]. The pore morphology, distribution, and connectivity of the shale were characterized using FE-SEM and FIB-SEM techniques, and it was concluded that many pores below 5 nm were developed [15]. Fluid invasion methods mainly include the gas adsorption method and the high pressure mercury intrusion method (HPMI). Using CO_2 adsorption, N_2 adsorption, CH_4 isothermal adsorption, and HPMI, the pore structure of Longmaxi Formation shale in southeast Sichuan was characterized by full pore size, and the control of pore structure on shale gas content was clarified [16]. Nonfluid intrusion methods mainly include nuclear magnetic resonance, micro-nano-CT, and small-angle X-ray scattering [17–19]. The pore characteristics and connectivity of the Longmaxi Formation shales in the Jiaoshiba area of the Sichuan Basin were evaluated using nano-CT and 3D reconstruction techniques. It was concluded that the shale pores are highly inhomogeneous and have good connectivity in general [20]. The analysis of the pore structure of multiple sets of shale in North America using HPMI, N_2/CO_2 gas adsorption, and SANS/USANS shows that the measurement results of shale pores by SANS/USANS and N_2/CO_2 gas adsorption methods are in good agreement [21].

In this study, the mudstone of the Qigequan Formation of the Quaternary in the Sanhu Depression of the Qaidam Basin is taken as the research object. Through SEM, gas adsorption, and HPMI, the pore structure characteristics of mudstones of different lithofacies in Tainan, Sebei No. 1, and Sebei No. 2 gas fields are identified, and the influence of pore difference development on the mudstone reservoir space is analyzed. Ultimately, it will guide the optimal selection of mudstone reservoirs and biogas exploration and development in the study area.

2. Geological Setting

The Qaidam Basin is a Mesozoic-Cenozoic intermountain basin developed since the Indo-China Movement. The formation of the Quaternary System is the product of the overall migration of the sedimentary center from west to east under the action of neotectonic movement at the end of the Tertiary [22]. The Sanhu Depression is located in the southeastern part of the Qaidam Basin. Under the action of the Late Himalayan Movement, the sedimentary center of the basin migrated from west to east, forming the Quaternary subsidence and deposition center in the Sanhu Depression [23, 24]. The Sebei Gas Field is located in the second structural unit of the north slope of the Sanhu Depression and is the leading natural gas producing area in the Qaidam Basin (Figure 1).

The exploratory well in the Sanhu Depression reveals the Quaternary Qigequan Formation from top to bottom (Q_{1+2}), Shizigou Formation of Upper Tertiary (N_2^3), Upper Youshashan Formation of Upper Tertiary (N_2^2), Lower Youshashan Formation of Upper Tertiary (N_2^1), Upper Ganchaigou Formation of Upper Tertiary (N_1), Lower Ganchaigou Formation of Lower Tertiary (E_3), and Lulehe Formation of Lower Tertiary (E_{1+2}). The exploration practice has confirmed that the Qigequan Formation and Shizigou Formation are the biogas reservoirs in the Sanhu area and the main exploration intervals at present [25].

Therefore, this paper only studies the mudstone of the Qigequan Formation. The mudstone of the Qigequan Formation of Quaternary is in the early diagenetic stage. The lithology is mainly light gray mudstone and sandy mudstone, with light gray siltstone, argillaceous siltstone, fine sandstone, thin calcareous mudstone, and grayish-black carbonaceous mudstone, and various lithologies frequently interact with each other.

3. Sampling and Laboratory Methods

The 30 samples selected in this study are mudstones from the Tainan, Sebei No. 1, and Sebei No. 2 gas fields. The samples used are located in the K7 to K9 interval of the Qigequan Formation. The TOC and mineral composition analysis of mudstone is carried out by organic carbon analyzer and X-ray diffraction analyzer.

3.1. SEM. The SEM image was taken by the Institute of Geology and Geophysics, Chinese Academy of Sciences. The instrument was a Zeiss SUPRA 55 Sapphire SEM. The diameter of the mudstone sample was 0.5~3.0 cm, and the thickness was 0.2~1.0 cm. The mudstone samples were cut into flakes and then observed by instruments. Firstly, the surface of each sample was mechanically polished, and then, the surface of mudstone samples was ground by argon-ion for two hours on Hitachi IM4000 equipment to remove uneven parts and surface attachments. SEM images can intuitively provide information such as pore morphology and pore structure parameters.

3.2. N_2 Adsorption. When the relative pressure (P/P_0) is 0.01~1, the N_2 adsorption experiments can test the pore size distribution, surface area, and pore volume parameters for pore sizes from 0.3 nm to 200 nm pores. Before the experiment, the mudstone sample was ground into 200 mesh and
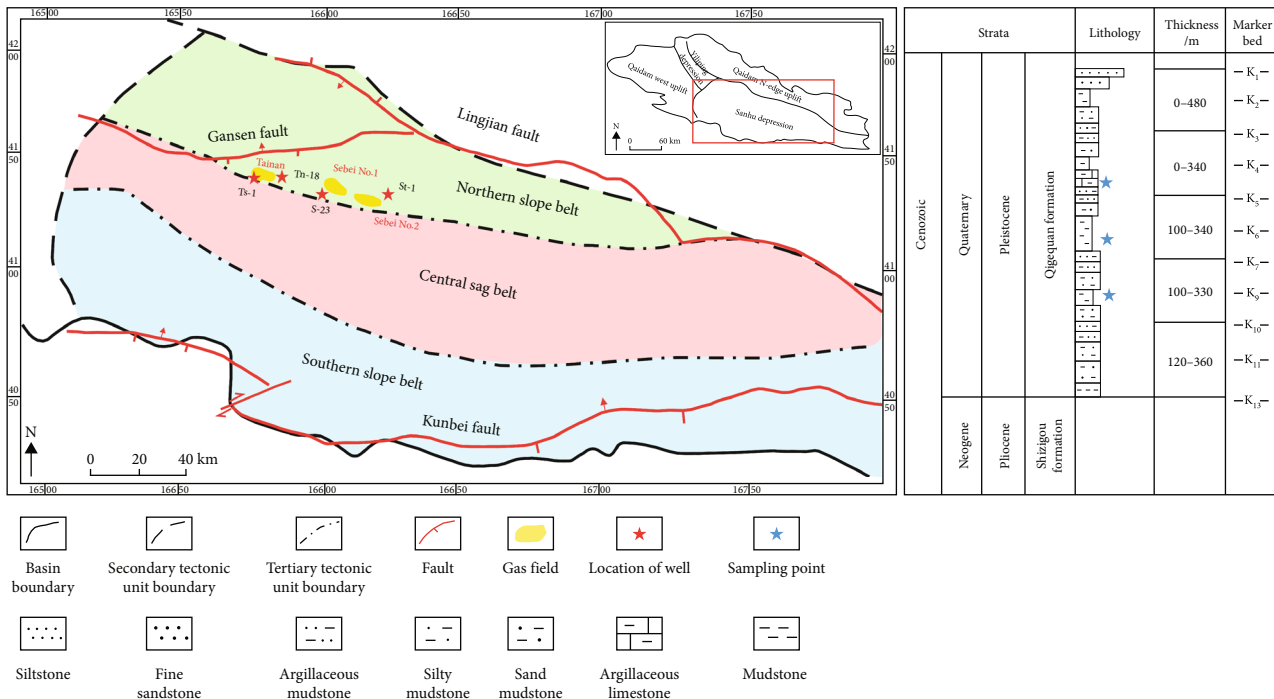
FIGURE 1: The structure of the Sanhu Depression and the histogram of Quaternary stratigraphy. Sanhu Depression is divided into the southern slope belt, central sag belt, and northern slope belt. The gas field is located in the northern slope belt. The experimental samples were taken from wells Tn-18, Ts-1, St-1, and S-23.

then dehydrated for five hours and degassed for 24 h at 110°C. The isothermal adsorption-desorption experiment was completed at 77.35 K.

3.3. HPMI. HPMI can characterize macropore size distribution and pore volume distribution of mudstone samples. The instrument is an AutoPore IV 9500 automatic mercury porosimeter produced by Mac Company. The samples were dried at 60°C for 48 hours before the experiment, then underwent vacuum treatment, after meeting the requirements of the HPMI. According to the injection volume of the Washburn equation under different pressures, the pore volume of varying pore sizes can be obtained.

3.4. TOC. Total organic carbon (TOC) content was determined by an ELTRA CS 800 carbon-sulfur analyzer, and the samples were pulverized to a particle size of about 0.12 mm before analysis. After the first weighing, the carbonate minerals in the samples were treated with dilute hydrochloric acid, and the second weighing was performed. After rinsing and drying, the samples were reweighed, and the TOC was obtained by calculating the mass of the samples before and after combustion and the amount of carbon dioxide generated after high-temperature combustion.

4. Results

4.1. Lithological Characteristics. According to the results of the TOC analysis (Table 1), the TOC value of mudstone samples is 0.06%~0.23%, with an average of 0.13%, indicating the abundance of organic matter in the study area is

extremely low. XRD results show that the mudstone samples in the study area are mainly quartz, feldspar, clay minerals, and carbonate minerals. The quartz content of mudstone samples is 25.36%~62.53%, with an average of 38.35%. The clay mineral content is 13.29%~38.42%, with an average of 26.56%. The feldspar mineral content was 13.60%~23.73%, with an average of 18.38%. The carbonate mineral content is 2.57%~23.63%, with an average of 15.44%. The Quaternary strata in the Sanhu Depression are thin interbeds of sandy and argillaceous sediments from top to bottom and generally have longitudinal and lateral heterogeneity. Quaternary mudstone can be divided into pure mudstone, silty mudstone, and sandy mudstone according to the size and relative content of mineral particles.

The pure mudstone is gray or dark gray as a whole, with extremely thin organic interlayers, and some layers are rich in bioclasts. Horizontal bedding is more developed. The pores are difficult to observe under the optical microscope. The silty mudstone has horizontal bedding, and microfractures are developed under the microscope. The grains are mainly quartz and feldspar, and micron-scale intergranular pores can be seen. Sandy mudstone is poorly cemented and easily fractured. The overall color is mainly light gray. The core particles are relatively coarse, the horizontal bedding is not developed, and most of them are massive structures. Under the microscope, it can be observed that the sandy particles are distributed in bands, and the particles are mainly quartz and feldspar. The interstitial material is mainly muddy, with a content of about 25%, mixed with a small amount of calcite. The rock contains powdered pyrite, partially agglomerated into lumps. Intergranular pores are

TABLE 1: TOC and mineral content of Quaternary mudstone samples.

Sample number	Depth (m)	TOC (%)	Clay (%)	Quartz (%)	Feldspar (%)	Carbonate (%)	Pyrite (%)	Lithology
H-1	1592.5	0.12	37.06	25.74	16.62	20.16	0.30	Pure mudstone
H-2	1596.4	0.15	35.56	30.60	14.08	19.01	0.60	Pure mudstone
H-3	1597.0	0.18	34.80	27.47	15.94	20.11	1.50	Pure mudstone
H-4	1589.3	0.23	22.10	37.04	20.60	19.43	0.60	Silty mudstone
H-5	1596.8	0.12	29.80	42.08	13.80	13.92	0.28	Silty mudstone
H-6	1852.0	0.17	28.89	37.62	19.47	11.95	1.90	Silty mudstone
H-7	1850.8	0.11	13.29	62.53	20.20	2.57	1.30	Sandy mudstone
H-8	1856.5	0.09	17.00	53.87	19.92	7.41	1.71	Sandy mudstone
H-9	1594.8	0.12	21.78	38.10	19.35	19.57	1.08	Silty mudstone
H-10	1595.0	0.16	26.31	29.83	20.92	22.13	0.65	Silty mudstone
H-11	1596.3	0.21	30.48	28.32	15.84	23.59	1.56	Pure mudstone
H-12	1596.5	0.08	32.80	27.50	16.71	21.49	1.42	Pure mudstone
H-13	1856.6	0.13	16.44	54.68	18.16	8.59	2.00	Sandy mudstone
H-14	1598.9	0.11	28.04	33.58	17.19	19.76	1.32	Silty mudstone
H-15	1599.3	0.15	28.93	38.31	18.77	11.98	1.86	Silty mudstone
H-16	1592.3	0.13	37.18	26.72	17.45	18.11	0.41	Pure mudstone
H-17	1851.0	0.21	35.61	30.49	14.16	19.07	0.46	Pure mudstone
H-18	1588.9	0.07	36.22	28.15	16.31	17.93	1.32	Pure mudstone
H-19	1589.2	0.16	24.30	33.10	22.53	19.29	0.62	Silty mudstone
H-20	1596.1	0.14	38.42	31.12	13.60	16.08	0.64	Pure mudstone
H-21	1599.2	0.12	26.76	38.72	19.79	12.93	1.68	Silty mudstone
H-22	1856.8	0.06	15.66	55.34	20.61	7.45	0.88	Sandy mudstone
H-23	1603.9	0.14	24.59	30.59	20.18	23.63	0.87	Silty mudstone
H-24	1851.7	0.07	14.64	51.45	23.73	9.68	0.43	Sandy mudstone
H-25	1590.1	0.09	26.86	35.70	16.33	19.96	1.06	Silty mudstone
H-26	1604.5	0.09	17.22	53.84	19.67	7.39	1.79	Sandy mudstone
H-27	1853.1	0.23	34.69	25.36	17.49	20.92	1.31	Pure mudstone
H-28	1604.6	0.06	13.95	56.48	20.84	7.22	1.45	Sandy mudstone
H-29	1605.0	0.10	19.44	51.59	18.43	9.41	1.03	Sandy mudstone
H-30	1855.5	0.13	27.95	34.61	22.67	12.54	2.10	Silty mudstone

developed in the sandy strips, which are characterized by poor connectivity (Figure 2).

4.2. Pore Morphology Characteristics. Many SEM experiments found that the pores of Quaternary mudstone reservoirs have significant heterogeneity on the microscopic scale, and as the observation scale decreases, the heterogeneity characteristics increase significantly. Previous research has done much research on mudstone pore morphology and classification [26–28]. Based on the classification of the contact relationship between pores and mineral components, a large number of rigid mineral intergranular pores, mineral intragranular pores, and clay minerals pores can be observed by SEM. The pore size ranges from nanometer to micron, providing ample storage space for free gas. A small amount of organic matter was observed, and the organic matter pores were relatively undeveloped (Figure 3).

4.2.1. Intergranular Pores of Rigid Minerals. The intergranular pores of rigid minerals are mainly developed between rigid minerals such as quartz, feldspar, pyrite, and calcite, which are triangle, strip, and irregular, and are one of the main types of Quaternary mudstone reservoirs [29]. The pore diameter is mainly distributed in the range of 20~500 nm, and the length of intergranular pores of rigid minerals can reach the micron level. These pores are generated with the burial depth and diagenesis of the mudstone, and they can be partially preserved under the conditions of more vital compaction and diagenesis due to the rigid mineral crystals such as quartz, feldspar, pyrite, and calcite, which have some resistance to compression.

4.2.2. Clay Mineral Pore. The Qigequan Formation mudstone mainly develops two types of pores related to clay minerals. Type I is related to pores developed along the bed of terrigenous clastic sheet clay minerals, and the shape of such
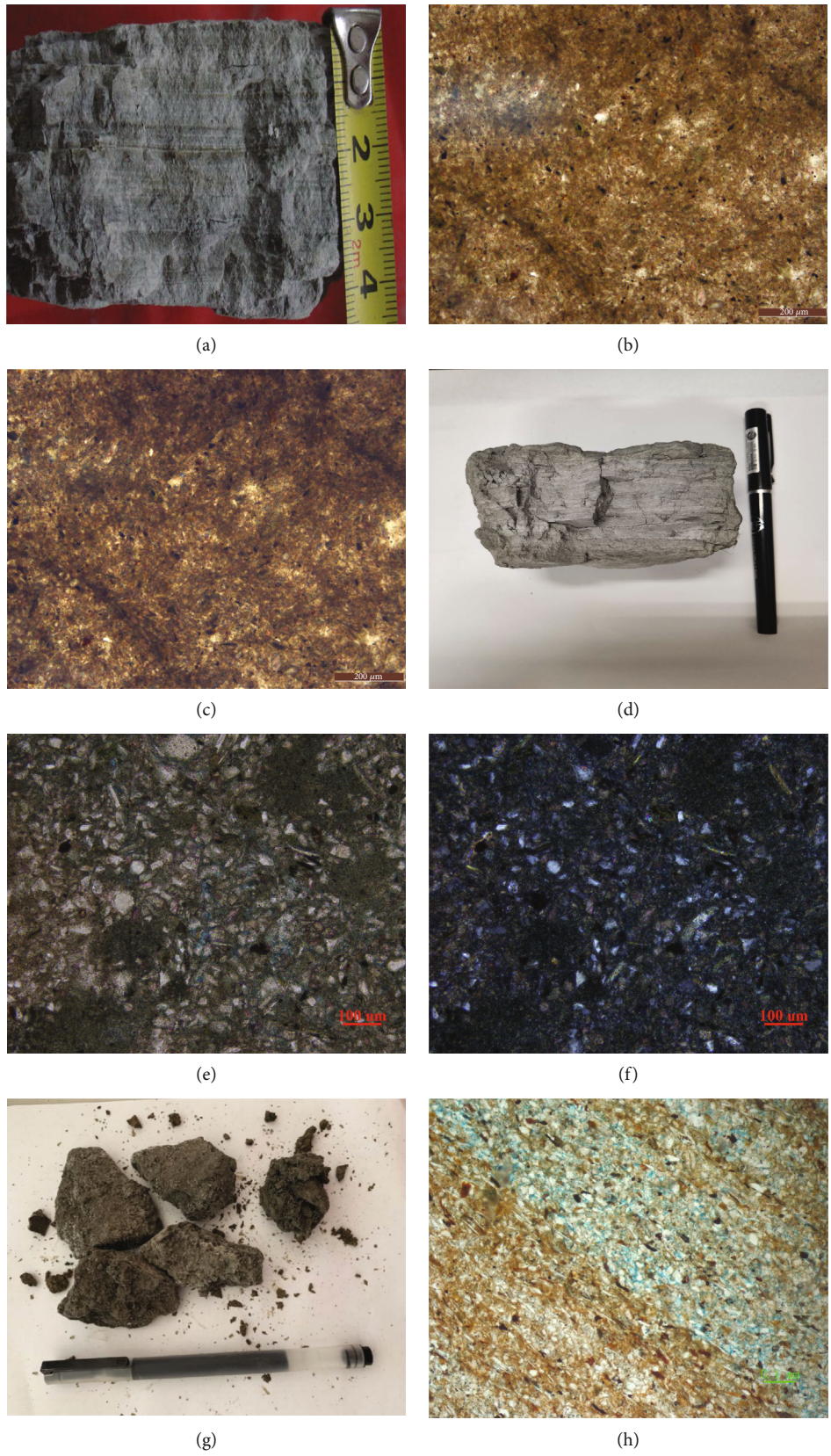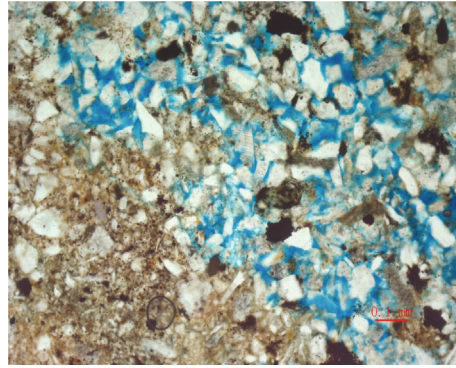
(a)

(b)

(c)

(d)

(e)

(f)

(g)

(h)

Figure 2: Continued.

(i)

FIGURE 2: Photos of cores and thin sections of mudstones of different lithofacies in the Qigequan Formation. (a) S-23: pure mudstone; horizontal bedding develops and sandwiches organic layers. (b) Tn-18: pure mudstone; pores are difficult to observe. (c) Tn-18: pure mudstone; pores are difficult to observe. (d) Tn-18: silty mudstone; horizontal bedding is developed and microfractures are visible. (e) Tn-18: silty mudstone; the grains are mainly quartz and feldspar, and a small number of pores can be seen. (f) Tn-18: silty mudstone; the grains are mainly quartz and feldspar, and a small number of pores can be seen. (g) Tn-18: sandy mudstone; the mudstone diagenesis is weak. (h) Ts-1: sandy mudstone; the sandy particles are distributed in bands, and the particles are mainly quartz and feldspar. (i) Ts-1: sandy mudstone; obvious intergranular pores are developed in the sandy belt.

pores is related to the distribution of clay minerals. Type II is the intercrystalline pores of clay minerals, which are formed by compaction and dehydration transformation between clay minerals. It is manifested as layered pores between clay mineral sheets or pores between clay mineral crystals [30]. The clay mineral pores are controlled by the direction of mineral crystal growth and are laminated primarily, with pore size generally ranging from 20 to 100 nm, which is more commonly developed. The pore development of clay minerals is concentrated, with complex cementation and poor sorting. The clay minerals have small particle sizes and strong plasticity, which are easy to transport after hydration and expansion, blocking the pore channel and reducing the permeability of the reservoir. The surface area of clay minerals is more significant than that of quartz and other minerals, and the more developed the clay mineral pores, the stronger the gas adsorption capacity. When the organic carbon content of the mudstone is low, the adsorption of clay minerals is very significant. Thus, it can be seen that clay mineral pores provide very considerable storage space for the Quaternary mudstone reservoir.

4.2.3. Intragranular Pores.
Controlled by geological action, quartz, feldspar, calcite, and other minerals in the mudstone are dissolved under the action of stratigraphic water, forming intragrain soluble pores [31]. In the SEM images of the Quaternary mudstone reservoir samples in the study area, more intragrain dissolution pores can be observed. It is mainly developed on the surface of carbonate mineral grains, and the intragrain soluble pores formed on the surface of quartz and feldspar grains are less common. The intragranular pores in the granules are mostly round and irregular polygons. Due to the weak compaction effect, the intragranular pores have not suffered compaction damage, and the development range of the intragranular pores within the granule ranges from nanometers to micrometers.

4.2.4. Organic Matter Pore.
Organic matter pores are irregular elliptical pores developed within organic matter due to hydrocarbon generation of organic matter [32]. Taking the marine shale of the Longmaxi Formation as an example, organic pores in shale are abundant, one of the most critical pore types [33]. However, organic matter pores are rarely developed in the Quaternary mudstone reservoirs, and only a tiny amount of organic matter pore development is observed in some samples of pure mudstone, which is not observed in silty mudstone and sandy mudstone. Because organic pores are controlled by the abundance and maturity of organic matter, the TOC of Quaternary mudstone ranges from 0.07% to 0.23%, and vitrinite reflectance of organic matter is mostly less than 0.5%. The organic matter content of the Quaternary mudstone is low and in the immature period, so it cannot meet the demand for organic matter pore development in large quantities.

4.3. Pore Distribution Characteristics

4.3.1. N$_2$ Adsorption.
According to IUPAC classification, the pore structure of pure mudstone and silty mudstone is the H3 type. The H3-type hysteresis loop is narrow, the adsorption curve is almost parallel to the desorption curve, noticeable capillary condensation occurs when the vapor pressure is close to saturation, and the adsorption curve rises sharply. It reflects the existence of parallel plate-shaped slit-type pores in the sample. Sandy mudstone has H4 type of pore structure, which represents a slit-type parallel plate-like pore structure. It also has the characteristics of some ink bottle pores and mainly develops rigid granular materials. This type of pores has a large adsorption hysteresis loop (Figure 4). On the whole, the Mesoporous pore structure of Quaternary mudstone in the Sanhu Depression is irregular, mainly with parallel-walled slit-type pores, as well as some cone-shaped flat holes, cone-shaped tube holes, and ink bottle holes. Many mesopores and macropores in the

(a)

(b)
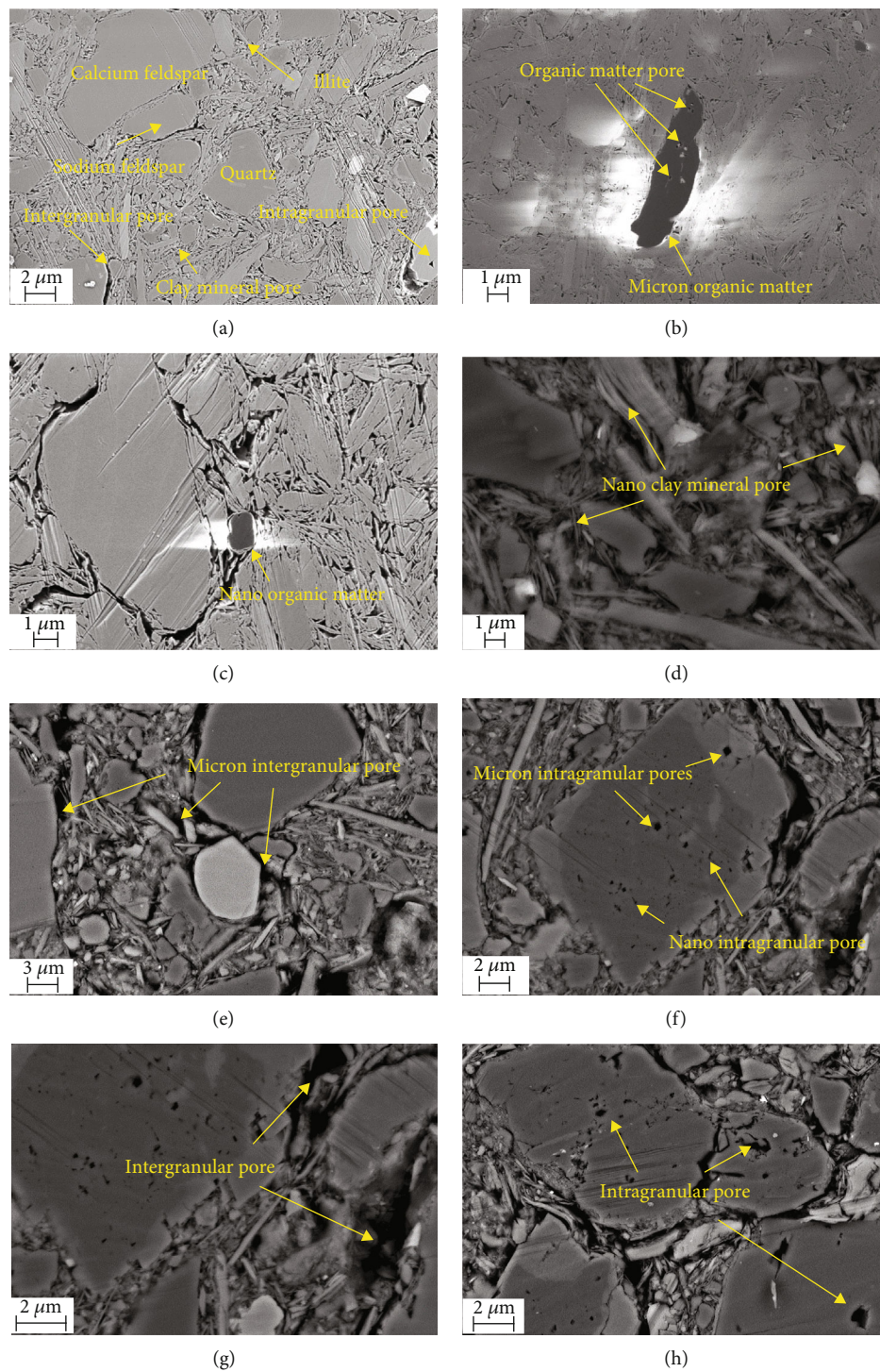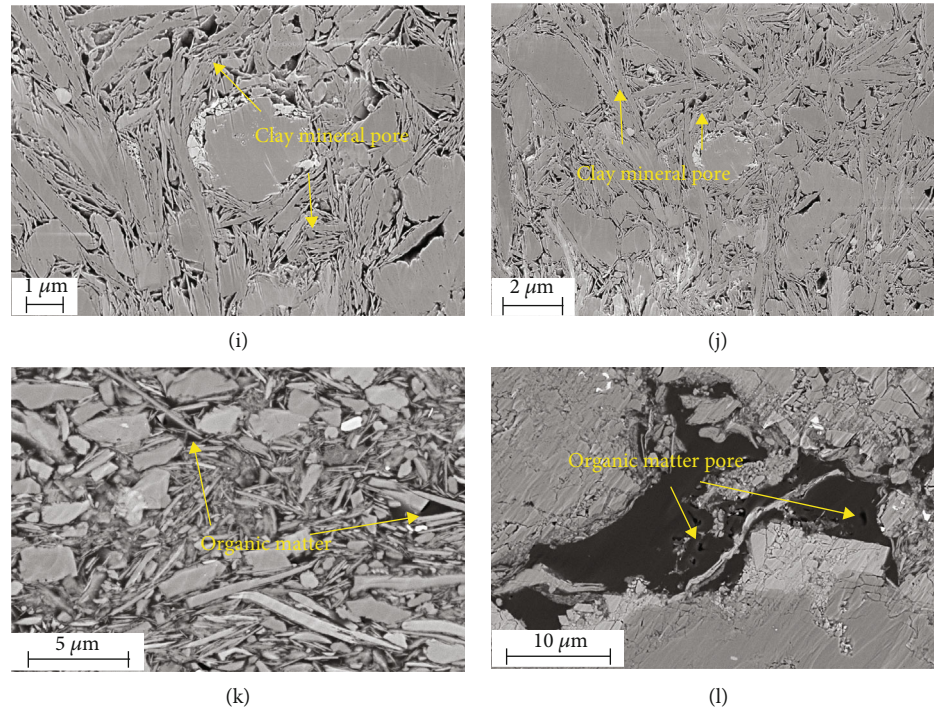
(c)

(d)

(e)

(f)

(g)

(h)

FIGURE 3: Continued.

FIGURE 3: SEM photographs of different types of pores in mudstone samples of the Qigequan Formation (by backscattered electron). (a) Tn-18: pure mudstone and the overall morphology characteristics of minerals and pores. (b) Tn-18: pure mudstone, micron organic matter, and organic matter pore. (c) Tn-18: silty mudstone and nanoorganic matter. (d) Tn-18: silty mudstone and nanoclay mineral pore. (e) Tn-18: silty mudstone and micron intergranular pore. (f) Tn-18: sandy mudstone and micro-nanointragranular pore. (g) Tn-18: sandy mudstone and intergranular pore. (h) Tn-18: sandy mudstone and intragranular pore. (i) Tn-18: pure mudstone and clay mineral pore. (j) Tn-18: pure mudstone and clay mineral pore. (k) St-1: pure mudstone and organic matter. (l) St-1: silty mudstone and organic matter pore.

mudstone are arranged in series, forming a complex pore throat system, and the pore structure is very complicated.

The distribution characteristics of pore volume and specific surface area change rate of mudstone are obtained by BJH and BET equations, respectively [34, 35]. It is found that the pore volume and specific surface area of mesoporous mudstone have similar distribution characteristics to pore size. The pore volume and specific surface area of mesoporous mudstone are mainly contributed by pores in the range of 5~20 nm (Figure 5). The pores in the range of 20~30 nm of individual samples also provide part of the pore volume and specific surface area, while the mesopores in the mudstone range have less contribution to the pore volume and specific surface area of mudstone. It shows that the pore volume and specific surface area of the Quaternary mudstone reservoir in the Sanhu Depression are mainly provided by pores of 5~20 nm (Figure 6).

4.3.2. HPMI. According to the typical characteristics of capillary pressure curves under different sorting and skewness summarized by Chilingar, mudstone shows various features (Figure 7). The threshold pressure of pure mudstone is the highest, ranging from 6.88 MPa to 9.64 MPa, with an average of 8.49 MPa, and the average maximum mercury saturation is about 76.58%. The sorting coefficient of pure mudstone is small, and the pore size distribution is relatively uniform. The threshold pressure of silty mudstone is high, ranging

from 0.41 MPa to 3.78 MPa, with an average of 2.04 MPa, and the maximum mercury saturation is about 85.22%. The sorting coefficient of sandy mudstone is significant, the flat section shown in the mercury injection curve is short, and the pore size distribution is uneven. The capillary pressure curve image of sandy mudstone tends to lower left, and the threshold pressure is relatively lowest, with an average of 0.06 MPa. The initial curve of mercury injection is gentle, indicating that the capillary pressure at this time corresponds to a relatively large number of pores controlled by the throat. A temporary flat section appears when the mercury intake reaches more than 15%, indicating more pores in this radius range.

The pore size distribution curve of mudstone based on HPMI shows that the rate of change of pore volume of Quaternary mudstone increases and then decreases with the growth of pore size (Figure 8). The pore volume of pure mudstone shows a bimodal phenomenon with the pore size distribution, mainly developing pore sizes 6~20 nm and 40~90 nm. The curves for pore sizes less than 100 nm vary significantly, which indicates that pores in the range of pore size less than 100 nm contribute considerably to the total pore volume. The pore volume of silty mudstone has a wide distribution with pore size, mainly in the range of 40-200 nm. Some samples have micron-scale pore development, indicating uneven pore size distribution. The pore size distribution of the sandy mudstone shows a single peak
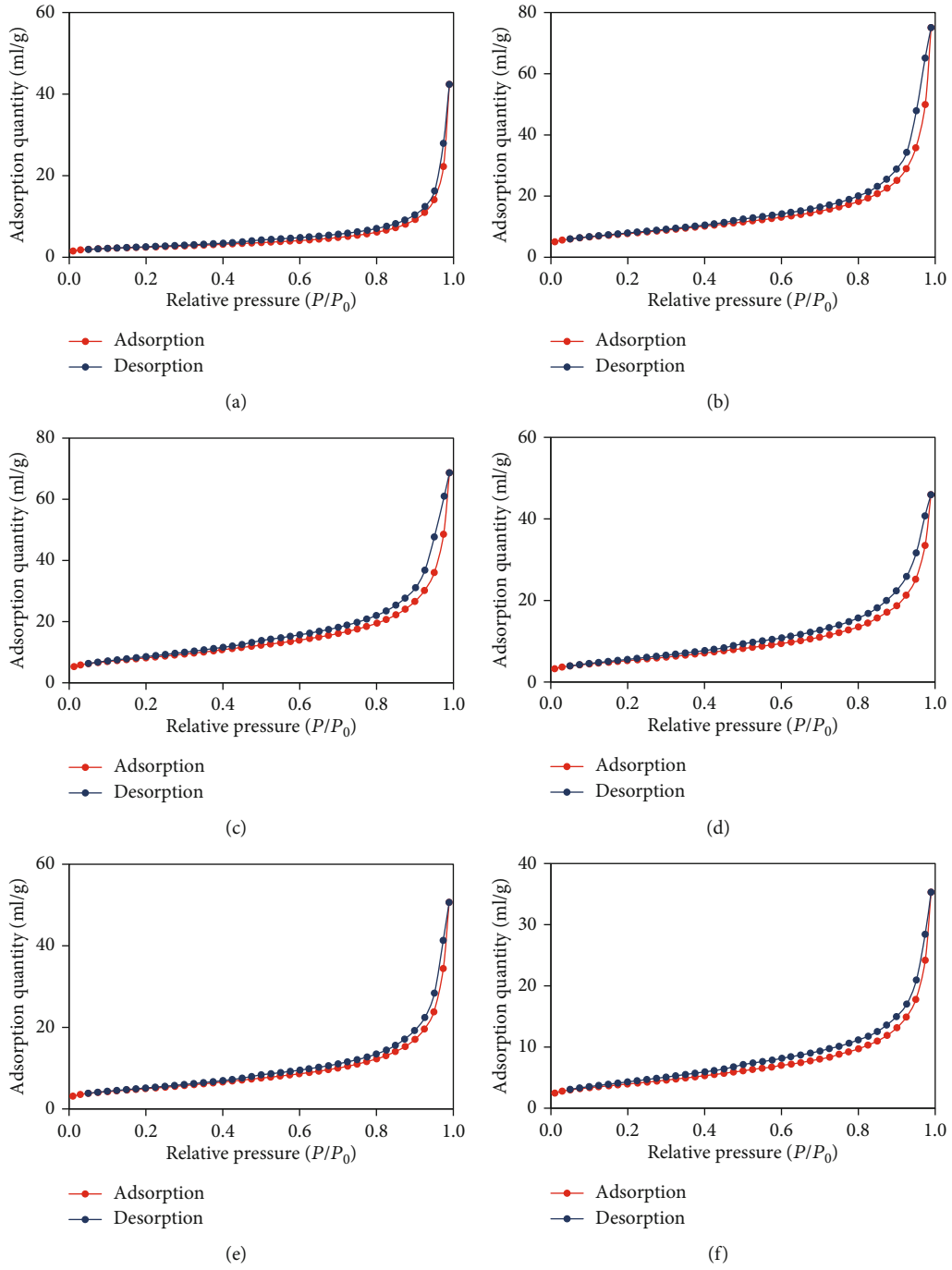
(a)

(b)

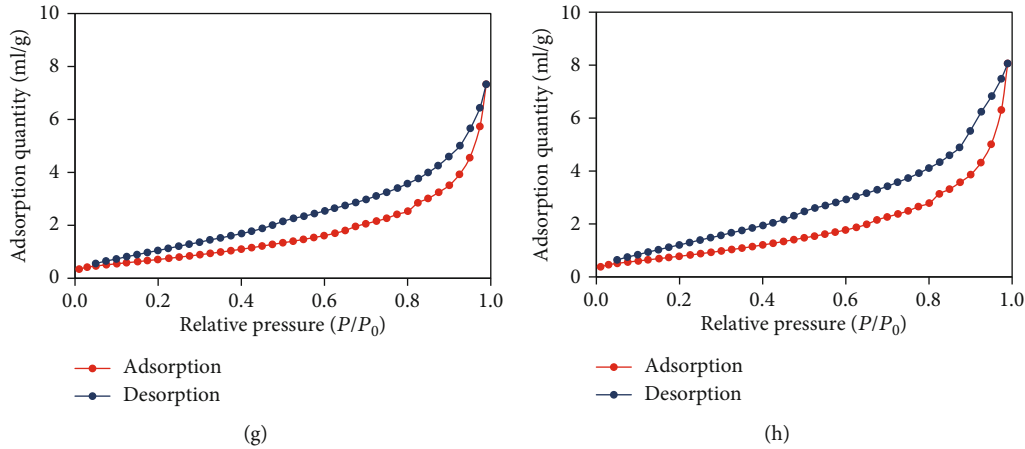(c)

(d)

(e)

(f)

Figure 4: Continued.

(g)

(h)

FIGURE 4: N_2 adsorption isotherms of different mudstones. (a) H-1: pure mudstone; (b) H-2: pure mudstone; (c) H-3: pure mudstone; (d) H-4: silty mudstone; (e) H-5: silty mudstone; (f) H-6: silty mudstone; (g) H-7: sandy mudstone; (h) H-8: sandy mudstone.

phenomenon, and a large number of pores with 10~20 μm pore size are developed. The pore volume with pore size distribution curves of different mudstone samples is inconsistent, indicating that the pores are strongly nonhomogeneous. The change rate of surface area decreases with the increase of pore size, and pores mainly contribute to the surface area of different mudstones within the pore size range of less than 30 nm (Figure 9).

5. Discussions

5.1. Whole-Aperture Distribution Characteristics. At present, domestic and foreign scholars have carried out many experimental studies on the whole-aperture distribution characteristics of unconventional reservoirs. The leading technologies are as follows [36]: the gas adsorption technology and mercury injection technology are combined to determine the whole-aperture distribution characteristics of mudstone. According to the advantages of different characterization techniques, the pore distribution characteristics of micropores (<2 nm), mesopores (2 ~ 50 nm), and macropores (>50 nm) in Longmaxi Formation shale and North American shale reservoirs in southeastern Sichuan were obtained by CO_2 adsorption, N_2 adsorption, and HPMI [37]. Due to the shallow burial depth, weak diagenesis, and uncemented state, Quaternary mudstone in Sanhu Depression rarely has micropore development. Therefore, the authors only discuss the distribution characteristics of mesopores and macropores. According to the different pore size characterization ranges and accuracy of the two experimental methods, the N_2 adsorption experimental data were selected for the mesopores, and the HPMI experimental data were chosen for the macropores. Thus, the whole-aperture size distribution characteristics of mudstone are obtained.

The pore volume of the Quaternary pure mudstone reservoir can reach 0.08~0.12 ml/g, with an average of 0.10 ml/g, and the main development pore size range is 6~90 nm. The proportion of macropore is 42.21%~60.85%, with an average of 52.06%. The proportion of mesopore volume ranged from 39.15% to 57.79%, with an average

of 47.94%. The pore volume of silty mudstone is 0.12~0.15 ml/g, with an average of 0.13 ml/g. The main pore size range is 40~200 nm, and some samples develop micron pores. The proportion of macropore is 37.64%~84.62%, with an average of 61.06%. The proportion of mesopore volume ranged from 15.38%~62.36%, with an average of 38.94% %. The pore volume of sandy mudstone can reach 0.23~0.24 ml/g, and the main developed pore size range is 0.5~10 μm. The proportion of macropore volume is 89.96%~96.26%, and the proportion of mesopore volume is 3.74%~10.04% (Table 2). The pore space is mainly contributed by macropores (Figure 10).

The surface area of the Quaternary pure mudstone reservoir is 14.75~28.27 m^2/g, and the average is 20.47 m^2/g. The surface area of mesopores is 83.49%~91.19%, and the average is 86.35%. The surface area of macropores is 8.81%~16.51%, and the average is 13.65%. The surface area of the silty mudstone reservoir is 9.55~23.17 m^2/g, with an average of 16.97 m^2/g. The surface area of mesopores ranged from 77.49% to 93.49%, with an average of 86.29%. The surface area of macropores ranged from 6.21% to 22.51%, with an average of 13.71% (Table 2). The sandy mudstone lacks mesopores, so the average surface area is only 7.68 m^2/g (Figure 11).

Compared with silty mudstone and sandy mudstone, pure mudstone has more mesopores and fewer macropores. The relatively high content of clay minerals in pure mudstones suggests that clay minerals are the main factor in the development of mesopores in Quaternary mudstones. In contrast, silty mudstones and sandy mudstones have higher contents of rigid minerals such as feldspar and quartz, indicating that the content of rigid minerals is the main controlling factor for macropore development. Rigid minerals are dominated by intergranular pores, intragranular dissolution pores, and cracks, so the pores associated with rigid minerals are relatively large. Mesopores also occupy an absolute advantage in the pore specific surface area, ranging from 65.71% to 93.49%, with an average of 83.49%. The contribution of macropores to the pore surface area of the pores is relatively tiny.
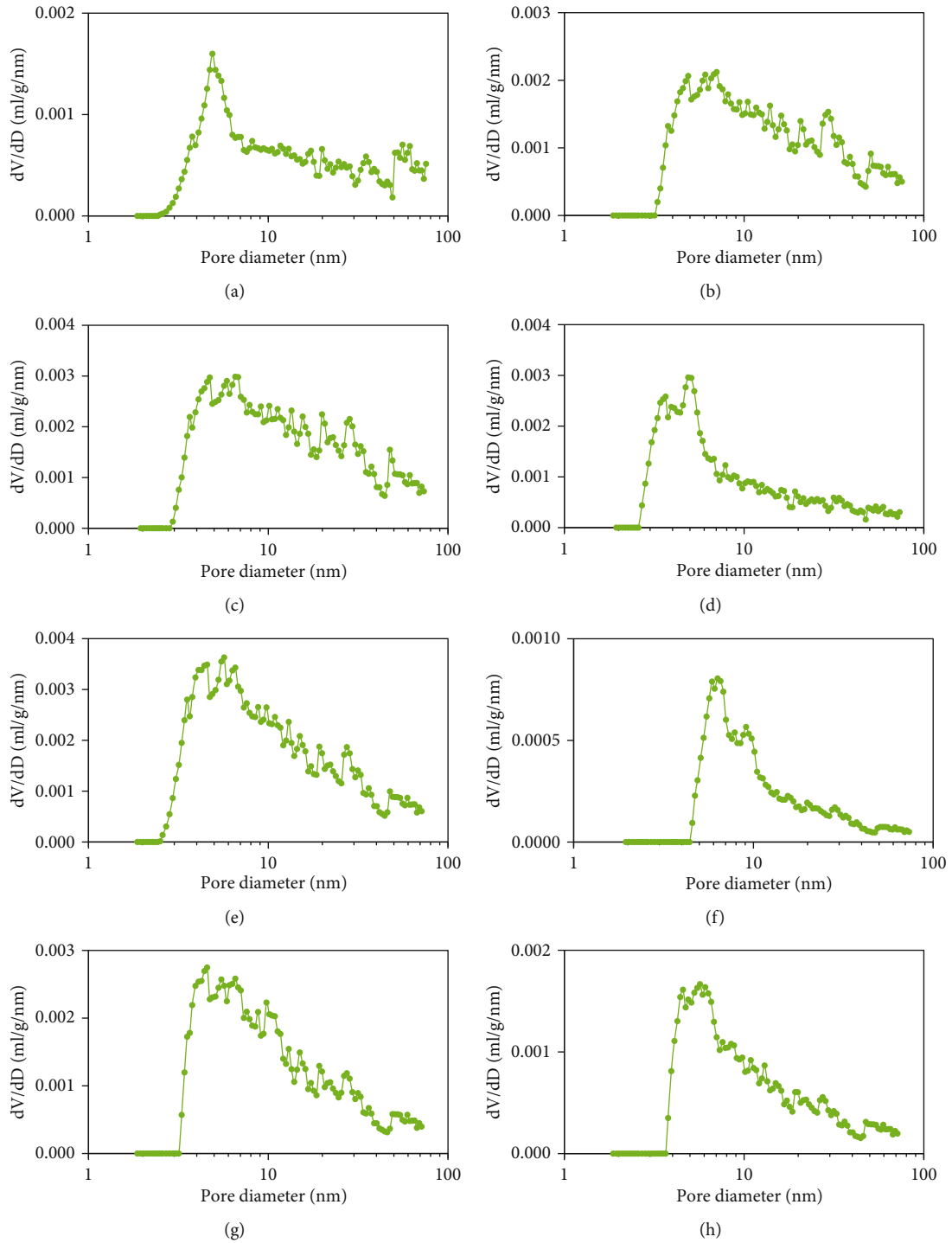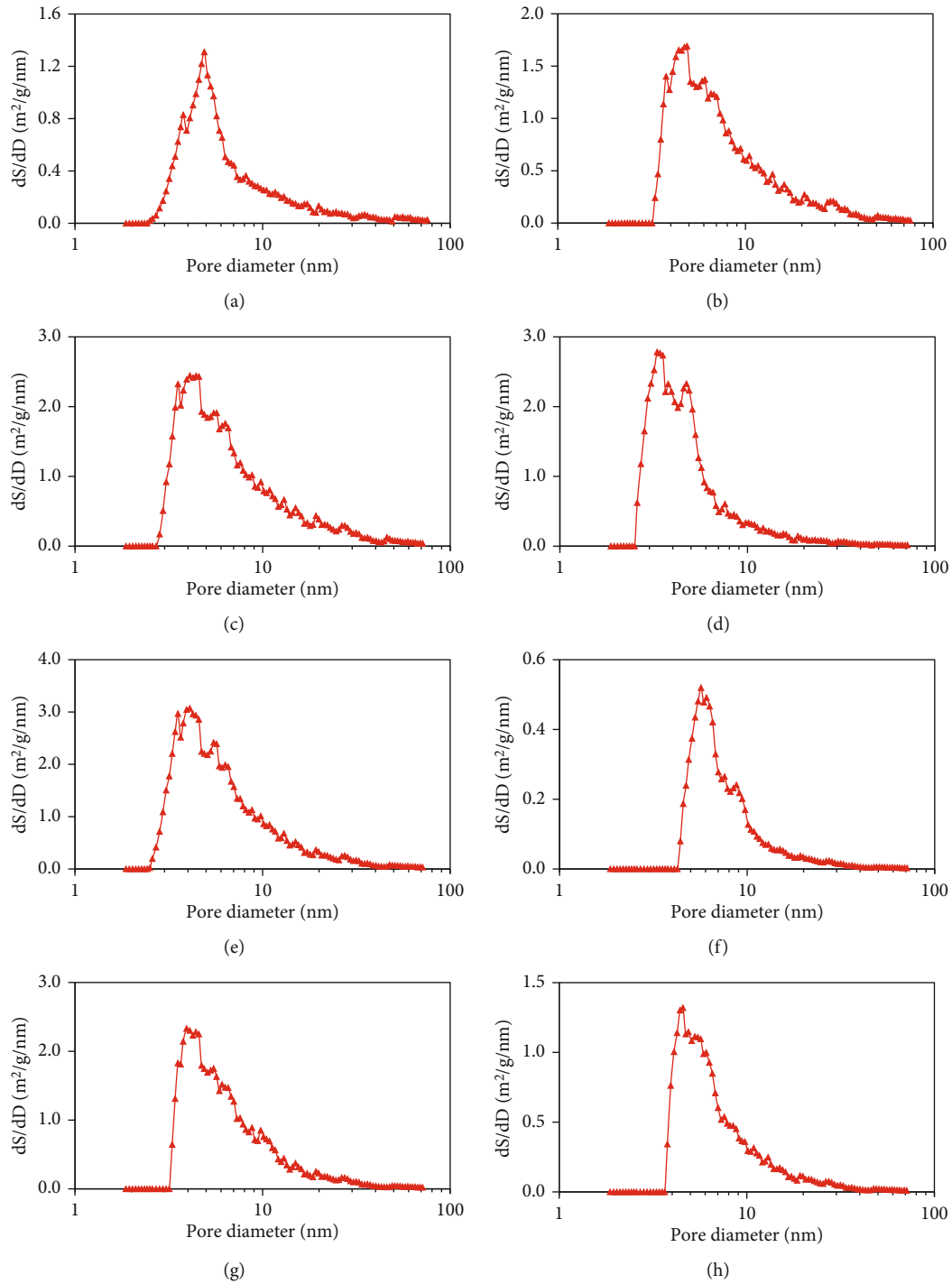
Figure 5: BJH desorption model pore volume distribution of Qigequan Formation mudstone samples. (a) H-1: pure mudstone; (b) H-2: pure mudstone; (c) H-3: pure mudstone; (d) H-4: silty mudstone; (e) H-5: silty mudstone; (f) H-6: silty mudstone; (g) H-7: sandy mudstone; (h) H-8: sandy mudstone.

5.2. Genesis of the Pore Structure of Mudstone Reservoir. The pore types in the mudstone are complex, so the development characteristics of micro-nanopores in mudstone reservoirs are comprehensively controlled by sedimentary diagenesis, mineral composition, organic carbon content, and thermal evolution degree of organic matter [38]. Some external and internal factors control the develop-

ment of the mudstone pore network. External factors include the influence of diagenesis on fluid properties, abnormal pressure generated during hydrocarbon generation, mineral transformation, and other factors. At the same time, the internal factors include organic matter abundance, thermal maturity, and mudstone composition, which are interrelated and have a significant impact

Figure 6: BET desorption model pore specific surface area distribution of Qigequan Formation mudstone samples. (a) H-1: pure mudstone; (b) H-2: pure mudstone; (c) H-3: pure mudstone; (d) H-4: silty mudstone; (e) H-5: silty mudstone; (f) H-6: silty mudstone; (g) H-7: sandy mudstone; (h) H-8: sandy mudstone.

on the pore network system [39]. A more detailed discussion on internal factors affecting pore structure is as follows.

5.2.1. Organic Matter. The pore network of the mudstone reservoir is composed of pores associated with organic matter and inorganic matter. Each mudstone reservoir has unique properties controlled by the amount of organic matter and minerals and thermal maturity. The reservoir quality depends on the pore structure, which relies on the development of primary and secondary pores, and the pores associated with organic matter are considered secondary pores [40]. Generally, organic matter content and maturity control the pore network in mudstone.
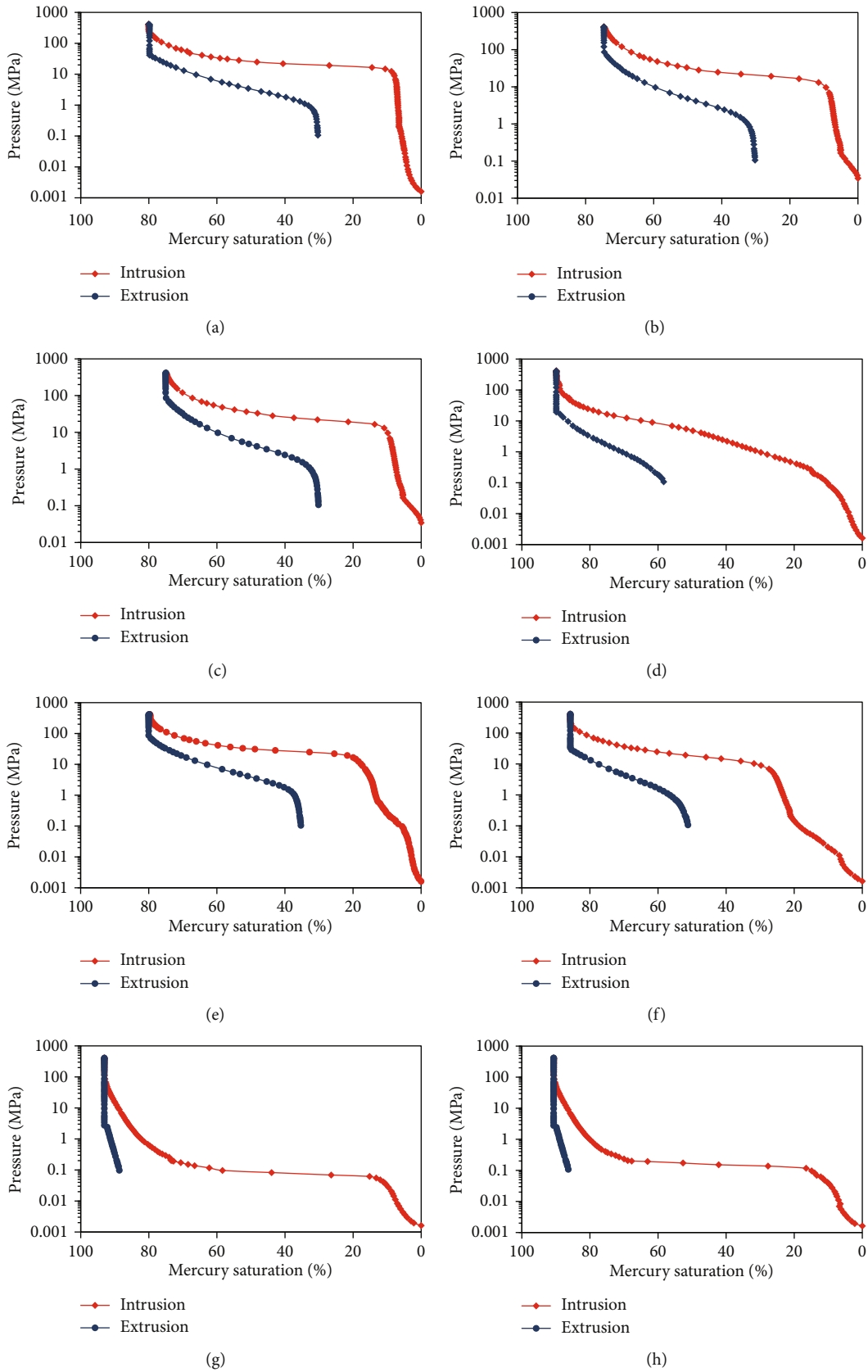
FIGURE 7: Capillary force curves of different mudstone samples. (a) H-1: pure mudstone; (b) H-2: pure mudstone; (c) H-3: pure mudstone; (d) H-4: silty mudstone; (e) H-5: silty mudstone; (f) H-6: silty mudstone; (g) H-7: sandy mudstone; (h) H-8: sandy mudstone.
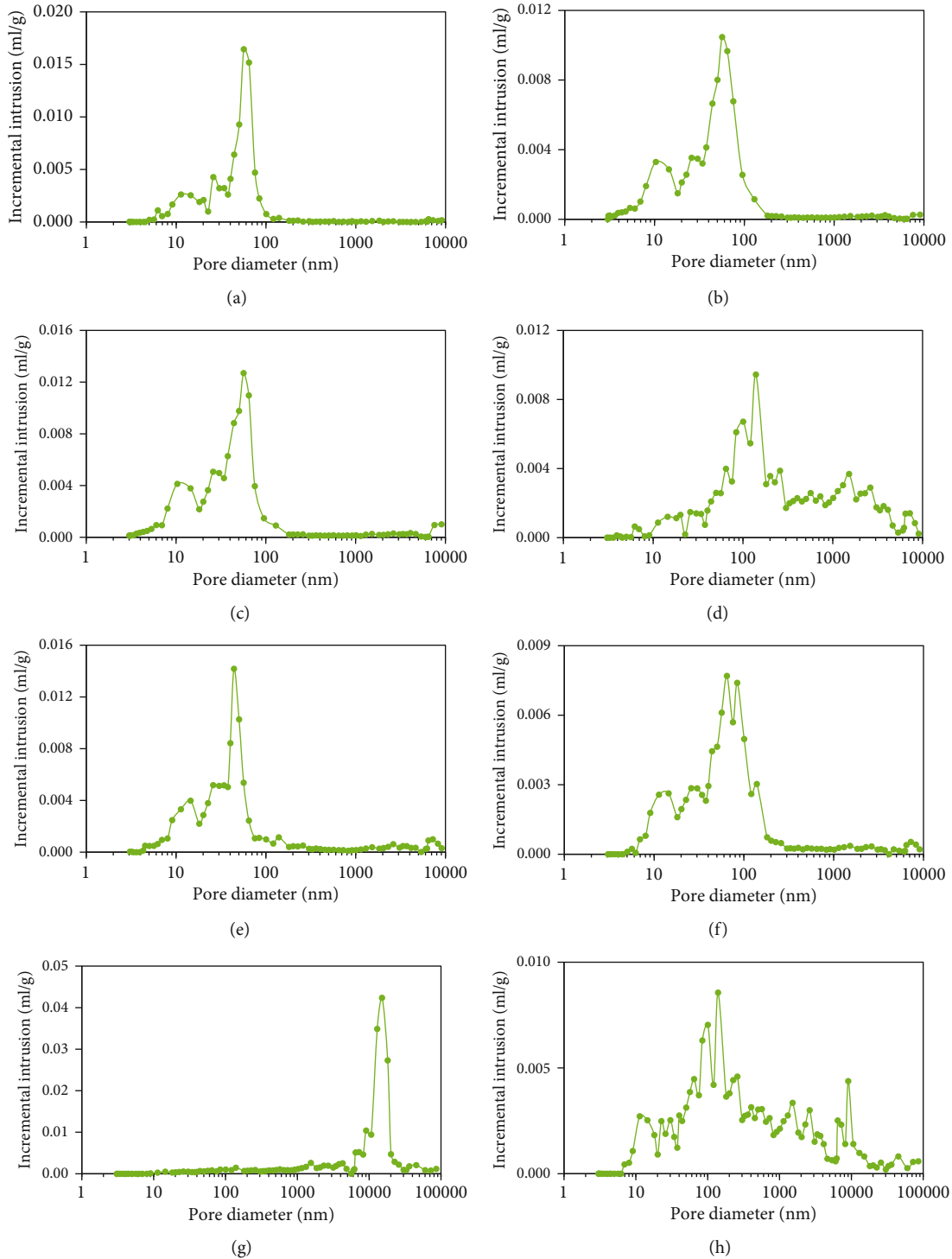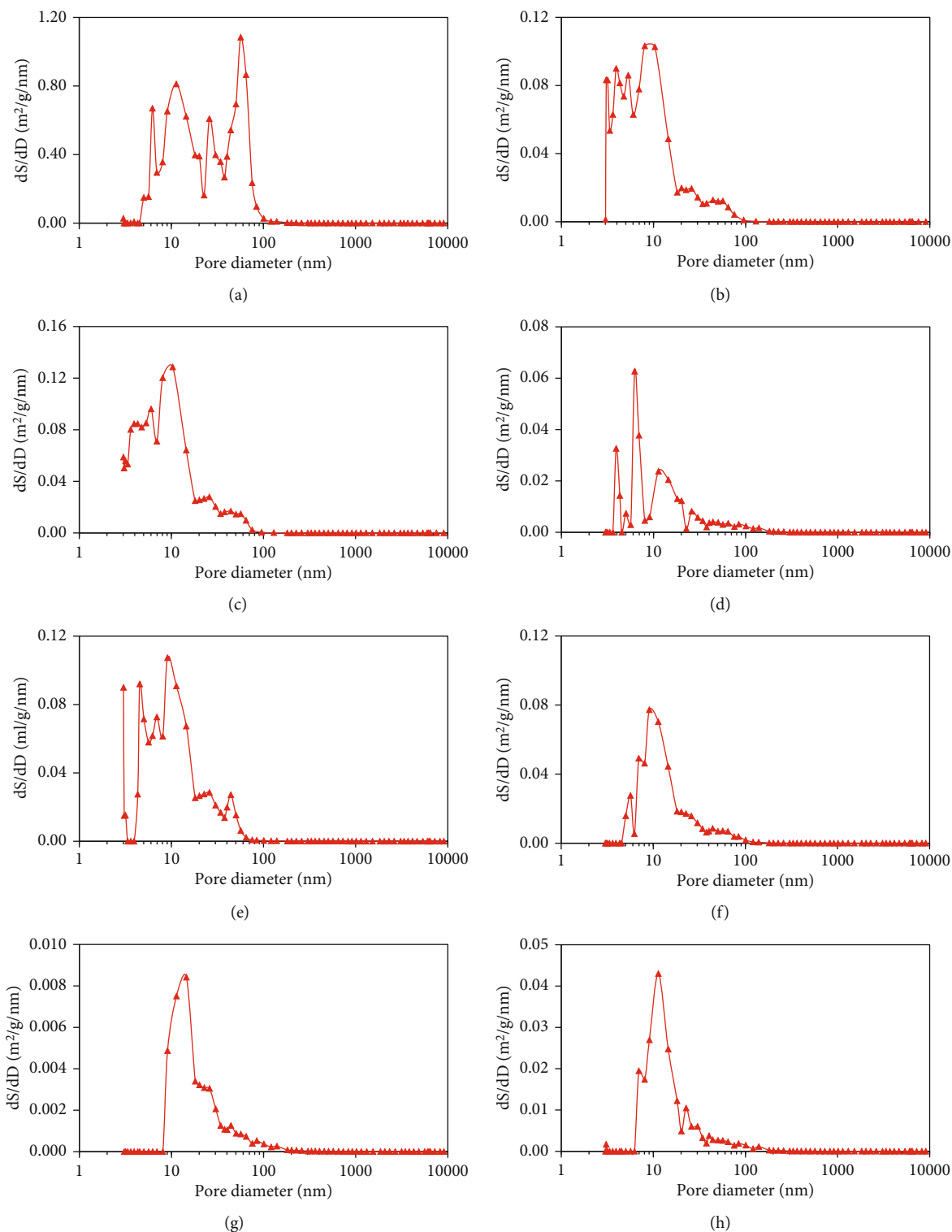
Figure 8: HPMI pore volume distribution of typical Qigequan Formation mudstone samples. (a) H-1: pure mudstone; (b) H-2: pure mudstone; (c) H-3: pure mudstone; (d) H-4: silty mudstone; (e) H-5: silty mudstone; (f) H-6: silty mudstone; (g) H-7: sandy mudstone; (h) H-8: sandy mudstone.

Through the correlation analysis between pore structure and TOC of Quaternary mudstone reservoirs in the study area, it is found that TOC has a reverse relationship or no apparent correlation with pore surface area and volume. The mesopore volume and surface area have a weak positive correlation with TOC ($R^2 = 0.0074$ and 0.0265), and the macropore volume and specific surface area have a weak negative correlation with TOC ($R^2 = 0.1215$ and 0.0185). It shows that TOC has no noticeable control effect on the development of

Figure 9: HPMI pore surface area distribution of typical Qigequan Formation mudstone samples. (a) H-1: pure mudstone; (b) H-2: pure mudstone; (c) H-3: pure mudstone; (d) H-4: silty mudstone; (e) H-5: silty mudstone; (f) H-6: silty mudstone; (g) H-7: sandy mudstone; (h) H-8: sandy mudstone.

mesopores and macropores that constitute the main body of pore surface area and volume (Figure 12). The Quaternary mudstone in the Sanhu Depression has low organic matter content and is in the immature stage. Organic matter has not reached a large amount of hydrocarbon generation to form micro-nanopores, so the effect of organic matter on the pore structure development of mudstone is weak.

TABLE 2: Pore volume and specific surface area of mudstone of Qigequan Formation.

Sample number	Pore volume (ml/g)		Surface area (m²/g)		The proportion of volume (%)		The proportion of surface area (%)	
	Mesopore	Macropore	Mesopore	Macropore	Mesopore	Macropore	Mesopore	Macropore
H-1	0.052	0.058	15.338	3.034	46.88	53.12	83.49	16.51
H-2	0.031	0.049	12.447	2.308	39.15	60.85	84.36	15.64
H-3	0.072	0.053	25.781	2.490	57.79	42.21	91.19	8.81
H-4	0.024	0.131	7.400	2.150	15.38	84.62	77.49	22.51
H-5	0.077	0.046	21.661	1.509	62.36	37.64	93.49	6.51
H-6	0.050	0.077	15.975	2.201	39.08	60.92	87.89	12.11
H-7	0.009	0.220	2.788	0.519	3.74	96.26	84.30	15.70
H-8	0.025	0.220	7.913	4.130	10.04	89.96	65.71	34.29
Average	0.042	0.107	13.663	2.293	34.30	65.70	83.49	16.51

5.2.2. Rigid Minerals. Rigid minerals are equivalent to skeletons in mudstone and provide large amounts of intergranular pores, including minerals such as quartz, feldspar, and carbonate. The results of the influence of rigid minerals on the pore structure development of the Quaternary mudstone are similar for quartz and feldspar. The volume of mesopores is weakly negatively correlated with the content of quartz and feldspar ($R^2 = 0.3651$ and 0.4862), and the volume of macropores is positively correlated with the content of quartz and feldspar ($R^2 = 0.7740$ and 0.6273). The surface area of mesopores is negatively correlated with both quartz and feldspar contents, and the surface area of macropores is not significantly associated with quartz and feldspar contents. The volume and surface area of mesopores are weakly positively correlated with carbonate mineral content ($R^2 = 0.2329$ and 0.2985). There is a negative correlation between macropore volume and carbonate mineral content ($R^2 = 0.6003$), and there is no significant correlation between macropore surface area and carbonate mineral content (Figure 13).

Rigid minerals such as quartz and feldspar easily form micron-level cracks after compression. At the same time, because rigid minerals such as quartz and feldspar can resist inevitable compaction, they can effectively retain part of the pores, providing space for mudstone reservoir pores and increasing pore volume. However, the contribution of the surface area of rigid minerals is not apparent or even inhibits the development of the surface area. The carbonate minerals in the study area have an evident influence on the mesopore and surface area of the mudstone. It may be that the acid fluid in the formation water of the study area acts on the carbonate rock to generate tiny dissolution pores and promote the development of mesopores.

5.2.3. Clay Minerals. Clay minerals have a unique layered crystal structure. Some pores are formed within the mineral particles, between the mineral particles, and between the crystal layers, which are usually ribbon, strip, plate, and flake [41]. The pore size distribution of pores of different types of clay minerals varies greatly, such as montmorillonite micropores are the most developed, ilmenite/montmorillonite

mixed level is the next, kaolinite develops medium to large pores, and illite and chlorite create micron-level pores.

The pore volume and surface area of the Quaternary mudstone reservoir are positively correlated with clay mineral content ($R^2 = 0.5418$ and 0.6141). There is a negative correlation between macropore volume and clay minerals ($R^2 = 0.9228$) and a weak positive correlation between macropore surface area and clay minerals ($R^2 = 0.0323$). The results show that clay minerals play an essential role in controlling the mesopore development of the main body of surface area and total pore volume (Figure 14). The pore size of the clay mineral pore in Quaternary mudstone reservoirs is mainly in the mesoporous range (<50 nm), so high clay mineral content promotes the development of mesopores and inhibits the growth of macropores. Clay minerals provide an important adsorption area for gas adsorption in Quaternary mudstone reservoirs without organic matter.

5.2.4. Compared with Marine Shale. Regarding the marine shale of the Longmaxi Formation in the Sichuan Basin, the development characteristics of shale pores are mainly controlled by TOC content, organic matter maturity, and mineral composition [42]. The TOC content of the marine shale of the Longmaxi Formation has a strong control effect on the pore volume and specific surface area, and the porosity is positively correlated with the TOC content. At organic matter maturity below 2.5%, porosity increases with thermal maturity but decreases with samples with higher thermal maturity. The porosity of organic matter and clay minerals tends to be preserved by the presence of rigid particles. These particles provide a framework that prevents these pores from collapsing. The porosity of marine shale framework minerals is mainly related to carbonate dissolution. The increase in the organic matter content of marine shale will lead to an increase in the content of micropores. Therefore, the micropores contribute a larger specific surface area. The carbonate mineral content can lead to an increase in the content of macropores [43].
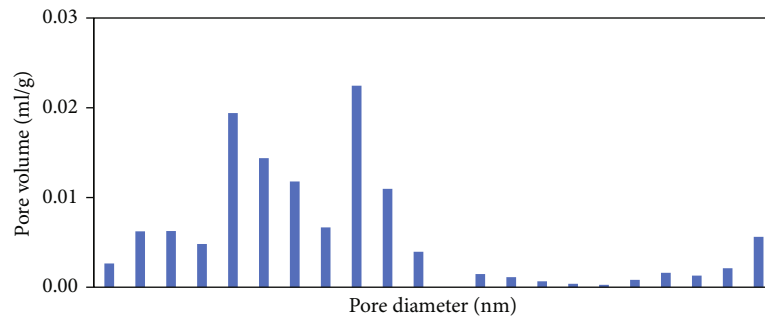
Compared with the marine shale of the Longmaxi Formation in Sichuan [44], the lacustrine mudstone of the Qigequan Formation in the Qaidam Basin has very different geological characteristics [43]. The TOC content
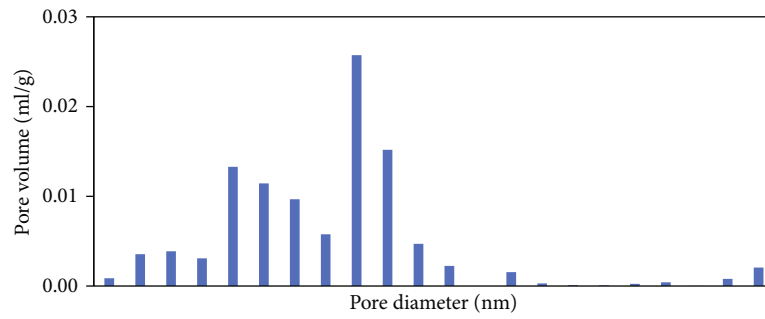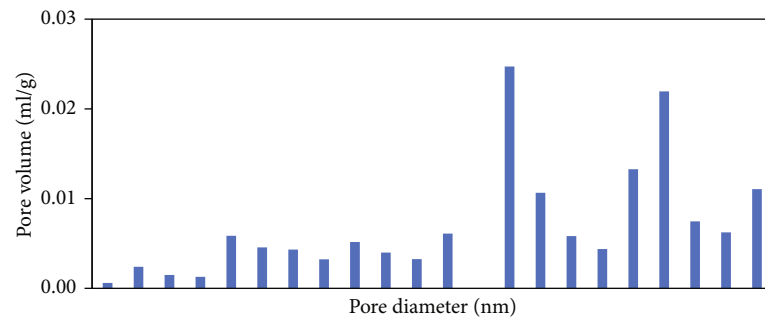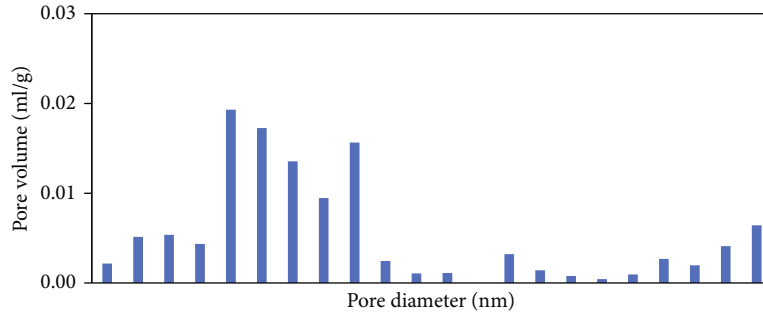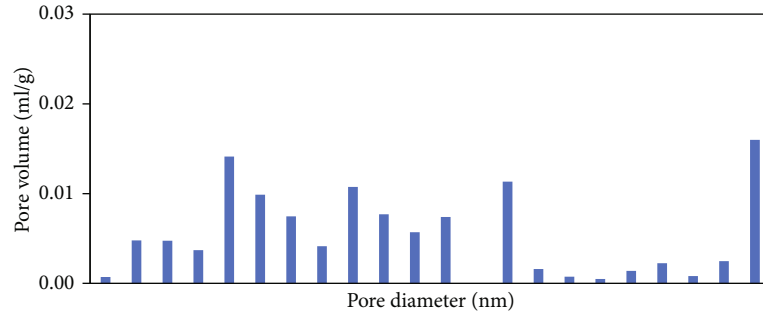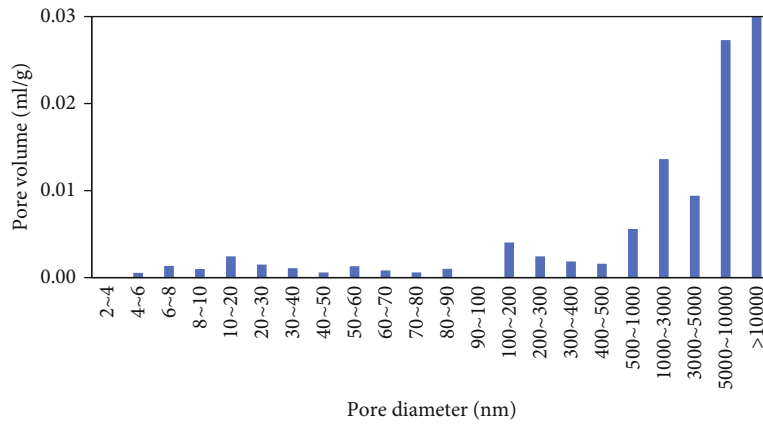
(a)
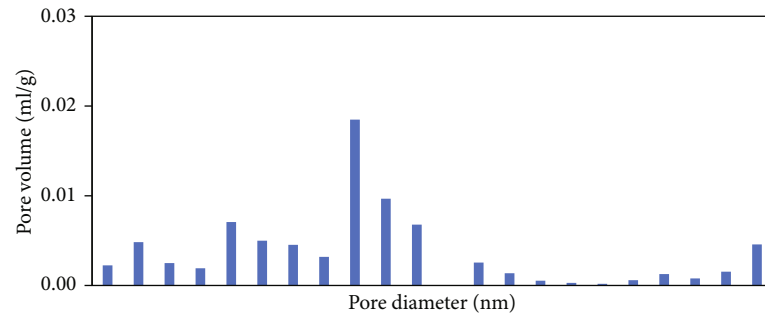
(b)
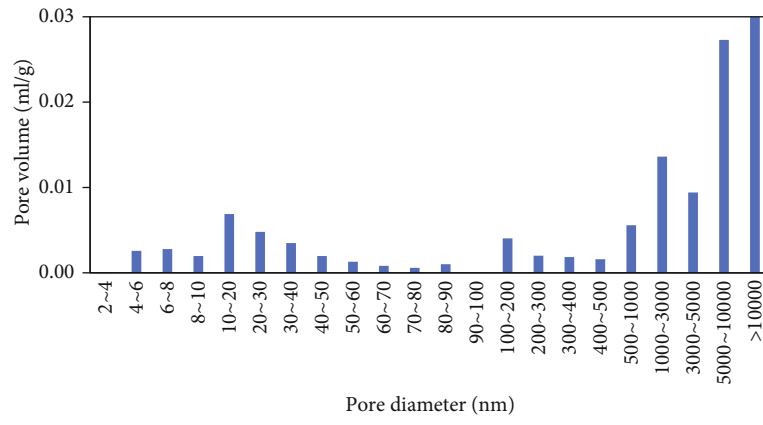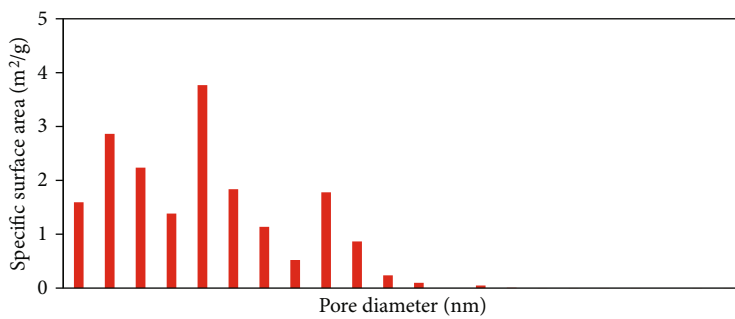

(c)

(d)

FIGURE 10: Continued.
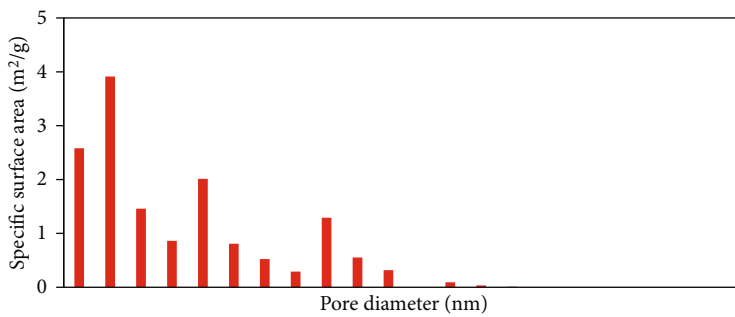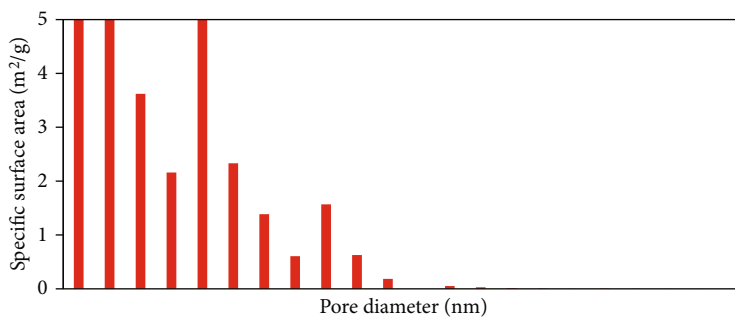
(e)

(f)

(g)

(h)

FIGURE 10: The pore volume distribution of mudstone in the Qigequan Formation. (a) H-1: pure mudstone; (b) H-2: pure mudstone; (c) H-3: pure mudstone; (d) H-4: silty mudstone; (e) H-5: silty mudstone; (f) H-6: silty mudstone; (g) H-7: sandy mudstone; (h) H-8: sandy mudstone.
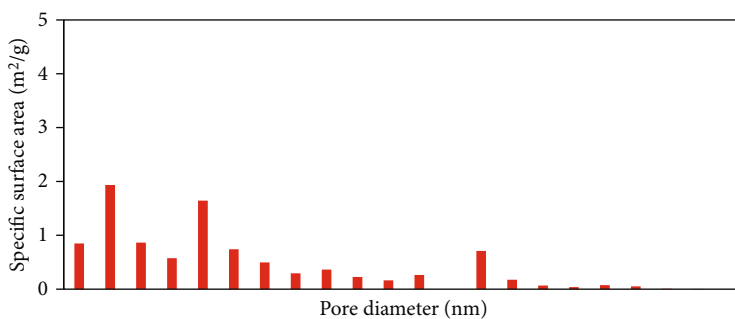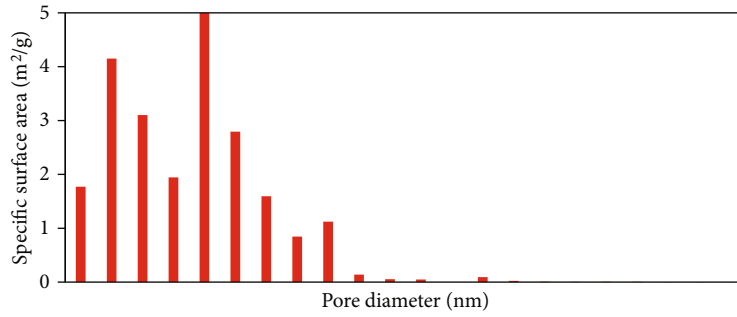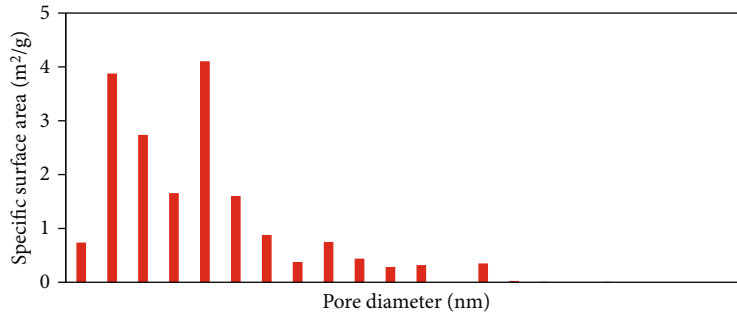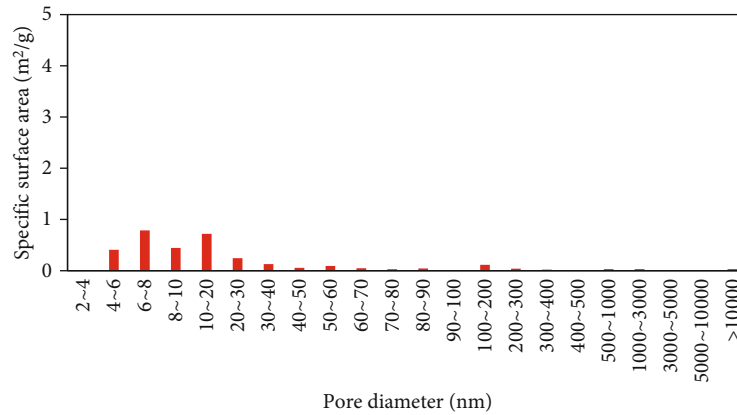
(a)

(b)

(c)

(d)
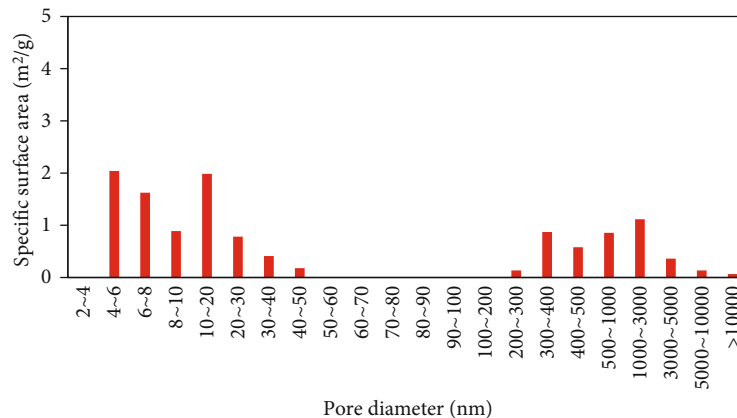
FIGURE 11: Continued.

(e)

(f)

(g)

(h)

FIGURE 11: The specific surface area distribution of mudstone in the Qigequan Formation. (a) H-1: pure mudstone; (b) H-2: pure mudstone; (c) H-3: pure mudstone; (d) H-4: silty mudstone; (e) H-5: silty mudstone; (f) H-6: silty mudstone; (g) H-7: sandy mudstone; (h) H-2: sandy mudstone.
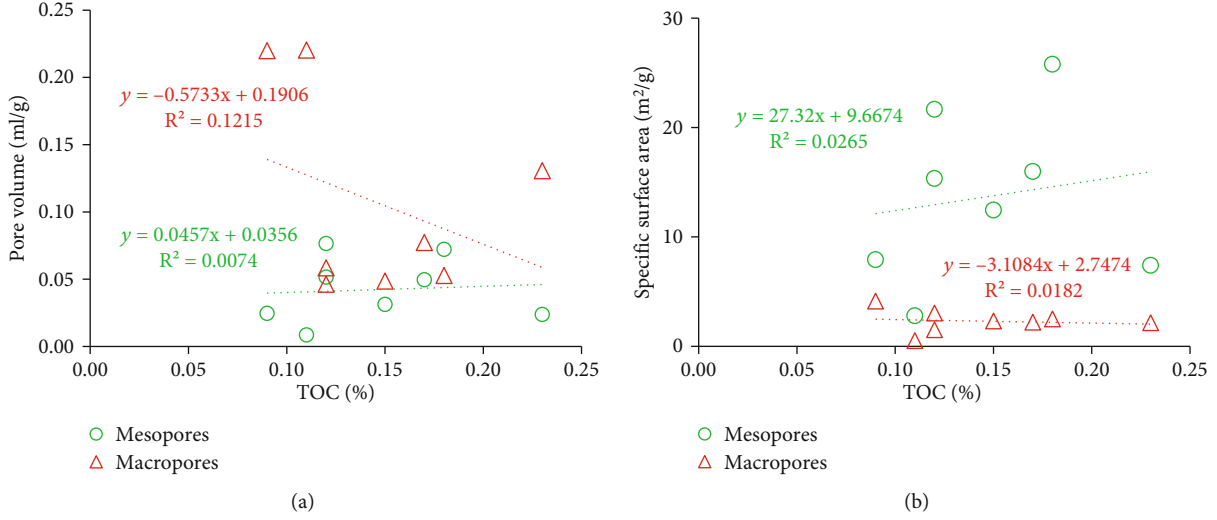
(a)

(b)

FIGURE 12: Plots showing the relationship between pore structure and TOC content. (a) Pore volume has a weak correlation with TOC; (b) no obvious correlation between specific surface area and TOC.

of lacustrine mudstone is low, and there is no obvious correlation between porosity and pore surface area, and TOC content. Because of the low TOC content and the degree of thermal evolution, the organic matter has not reached a large amount of hydrocarbon generation to form pores. Therefore, micropores related to organic matter are rarely developed. The lacustrine mudstone of the Qigequan Formation is characterized by relatively high clay mineral content. Clay minerals are the main factor for the development of mesopores, and the content of mesopores and specific surface area is significantly correlated with clay minerals. Similar to marine shale, lacustrine mudstone also has the feature that pores are preserved due to the existence of rigid mineral particles. Due to the weak diagenetic compaction in the later stage, there is an obvious correlation between macropores and the content of the rigid mineral particle.

5.3. The Controlling Effect of Pore Structure on Gas Migration. There are two basic types of natural gas migration: seepage and diffusion. The gas transmission mechanism in nanopores includes continuous flow, slippage flow, Fick diffusion, transition flow diffusion, and Knudsen diffusion [45, 46]. These migration types summarize the mechanism and power of mudstone gas migration and have their mechanism and control factors.

The average free path is the linear path between a molecule and other molecules through two successive collisions. According to the ideal gas collision theory, the average free path of gas molecules is [47]

$$\lambda = \frac{KT}{\sqrt{2}\pi d_m^2 P}, \qquad (1)$$

where λ is the average free path of gas molecules, m; K is a Boltzmann constant, J/K; T is the gas temperature, K; d_m is the diameter of the gas molecule, m; and P is gas pressure, Pa.

The Knudsen number is the ratio of the average free path of gas molecules to the characteristic length of objects in the flow field [48]. Generally, the Knudsen number is used to determine whether the fluid is suitable for the continuum hypothesis. The Knudsen number formula for mudstone gas migration is [49]

$$Kn = \frac{\lambda}{2r}. \qquad (2)$$

The transport mechanism can be divided into various forms according to the intensity of the interaction between the gas molecules of nanopores and the pore wall, namely, the Kn numerical range. The gas transport mechanism in the pores of mudstone at different scales is different, and the corresponding transport capacity is also different. When the pore diameter of mudstone is much larger than the free path of gas molecules, that is, Kn is less than 0.001, the gas migration form is Darcy seepage [50]. When the pore size of mudstone continues to decrease, the Kn number is between 0.001 and 0.01, the gas migration form is slippage seepage [51]. When Kn is between 0.01 and 0.1, the pore diameter is much larger than the average free path of methane gas molecules. At this point, the collision of methane gas molecules mainly occurs between free methane gas molecules, and the collision opportunities between molecules and capillary walls are relatively small. Such diffusion follows the Fick theorem, known as the Fick-type diffusion [52]. When Kn is between 0.1 and 10, the pore diameter is similar to the average free path of methane gas molecules, and the collision between molecules and the clash between molecules and the wall is equally essential. Therefore, the diffusion is a transition between Fick and Knudsen diffusion [53]. The pore size of mudstone decreases further, that is, Kn > 10, the characteristic value of gas migration is pore diameter, and the gas migration form is Knudsen diffusion [54].

(a)

(b)

(c)

(d)

(e)

(f)

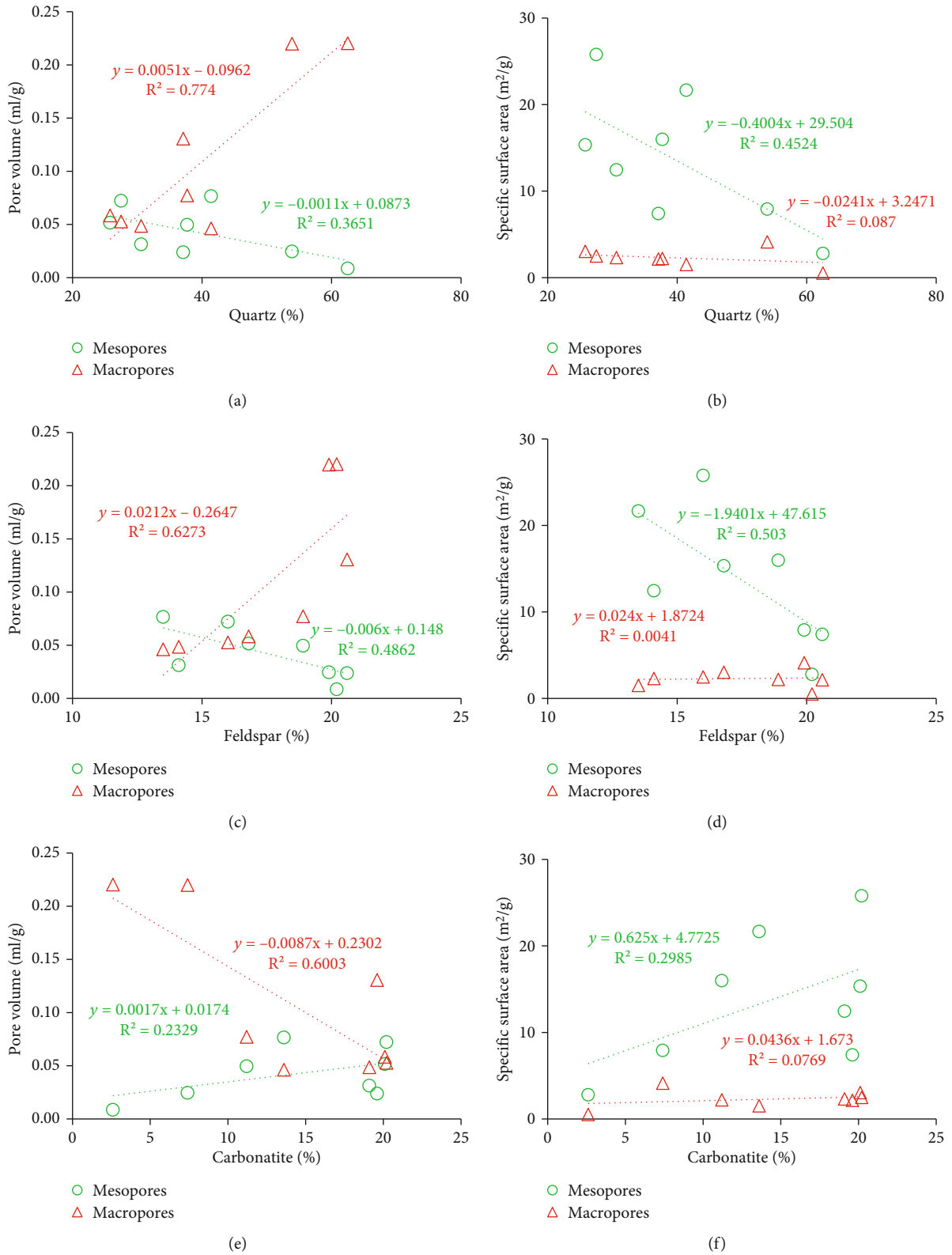FIGURE 13: Plots showing the relationship between pore structure and rigid mineral content. (a, c) Macropore pore volume is positively correlated with quartz and feldspar; (b, d) mesopore specific surface area is negatively correlated with quartz and feldspar; (e) macropore pore volume is negatively correlated with carbonate; (f) mesopore specific surface area has a weak positive correlation with carbonate.
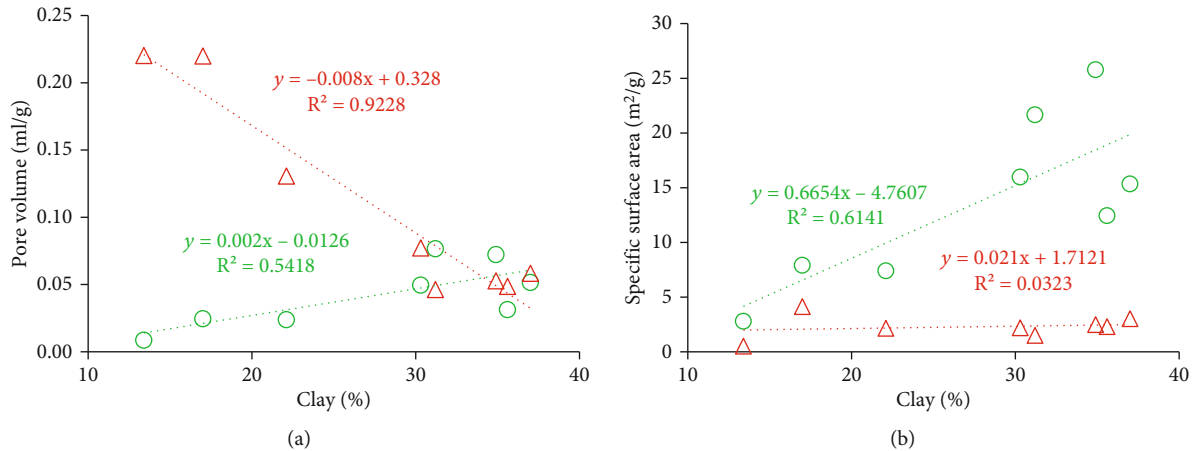
Figure 14: Plots showing the relationship between pore structure and clay mineral content. (a) Macropore volume has a negative correlation with clay; (b) mesoporous specific surface area is positively correlated with clay.

Based on the differential enrichment mathematical model of mudstone gas, based on the full-scale pore size distribution characteristics of mudstone reservoirs and combined with the critical conditions of mudstone gas diffusion and seepage in areas, the distribution interval and migration ability of mudstone full-scale pore size diffusion and seepage can be calculated. Based on the characteristics of the Quaternary mudstone gas reservoir in the Sanhu Depression (18 MP, 60°C), the different transport forms to the pore size range are Knudsen diffusion (<0.4 nm), transition flow diffusion (0.4 ~ 4.0 nm), Fick diffusion (4.0 ~ 40.0 nm), slippage flow (40.0~398.0 nm), and Darcy flow (>398.0 nm). The proportion of pore volume corresponding to different gas migration forms in pure mudstone reservoirs is 2.11%, 50.34%, 38.17%, and 9.37%. The proportion of pore volume corresponding to different gas migration forms in silty mudstone reservoirs is 0.64%, 40.86%, 44.65%, and 13.85%. The proportion of pore volume corresponding to different gas migration forms in sandy mudstone reservoirs is 0.00%, 3.97%, 5.65%, and 90.42%. Fick diffusion occurs in 50.34% and 40.86% of pore volume in pure mudstone and silty mudstone, and mesopores are the main diffusion space. The Darcy flow occurs in 90.42% of the pores of sandy mudstone, and the pores with pore size greater than 400 nm are the main space for Darcy flow (Figure 15).

From pore structure and gas migration control, the Quaternary mudstone reservoir has unique development characteristics. Compared with conventional reservoirs, Quaternary mudstone reservoirs also possess considerable pore volume (0.08~0.23 ml/g) and develop many nanopores. In particular, the percentage of mesoporous (<50 nm) pores in pure mudstone and silty mudstone can reach 47.94% and 38.94%, respectively. The massive development of nanopores causes the adsorption of mudstone medium and the binding of capillary force, which leads to the failure of long-distance migration of biogas. Many pores can only migrate in the form of Fick diffusion, the mudstone reservoir is in a "self-sealing" state, and biogas is generated and accumulated in situ. The "self-generation and self-storage"

accumulation characteristics of the Quaternary mudstone reservoir are not possessed by the conventional reservoir.

Compared with the tight reservoir, the surface area of some pure mudstone and silty mudstone can also reach 20 m²/g due to the development of many nanopores. The difference is that the surface area of tight reservoirs is mainly contributed by micropores and a small number of mesopores, while a large number of developed mesopores provide the surface area of Quaternary mudstone reservoirs. These mesopores can provide considerable surface area and contribute a lot of free gas enrichment space, which is the advantage of Quaternary mudstone reservoir development.

The particularity of the pore structure of the Quaternary mudstone reservoir creates its unique accumulation model. The pure mudstone reservoirs are mainly dominated by Fick diffusion and slippage flow, accounting for 50.34% and 38.17% of the pore volume, respectively, which have the characteristics of self-sealing enrichment and accumulation. The sandy mudstone reservoir is the coexistence of Fick diffusion, slippage flow, and Darcy flow, and the pore volume can reach 48.86%, 44.65%, and 13.85%, respectively. It shows the characteristics of both self-sealing accumulation and Darcy flow accumulation. The sandy mudstone is mainly Darcy flow, accounting for 90.42% of the pore volume. It has difficulty in self-sealing and only has Darcy flow enrichment characteristics.

Combined with the development characteristics of mudstone reservoirs, its controlling effect on gas accumulation is further analyzed. In the deep depressions of the Sanhu area, the porosity of mudstone gradually decreases with the deepening of strata burial. Mudstone forms a self-enclosed environment. The depth of 1500 m is the peak area of gas production by methanogens, and the amount of methane generated is far greater than the amount of gas diffusion and loss, forming a self-sealing overpressure mudstone biogas reservoir. In the slope zone of the Sanhu area, groundwater is continuously replenished by the melting water of ice and snow in the Kunlun Mountains, resulting in the overall water saturation of mudstone reaching more
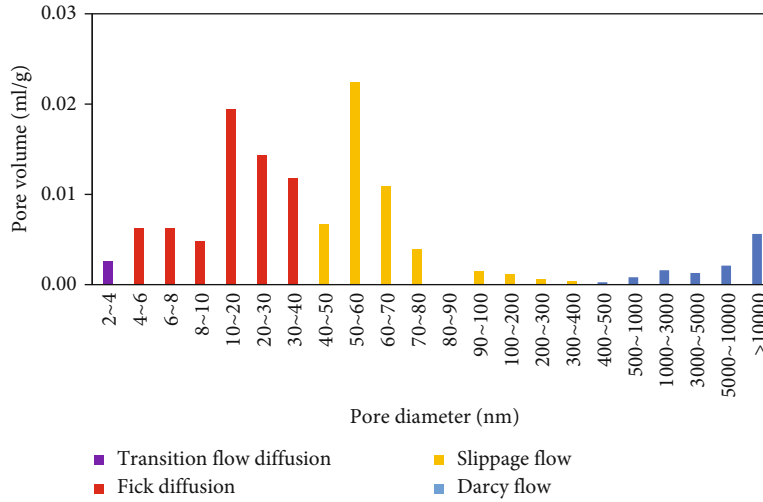
(a)
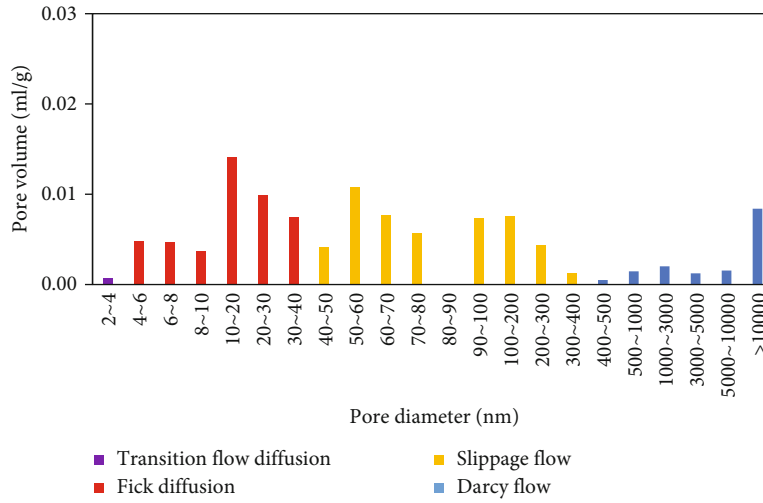
(b)
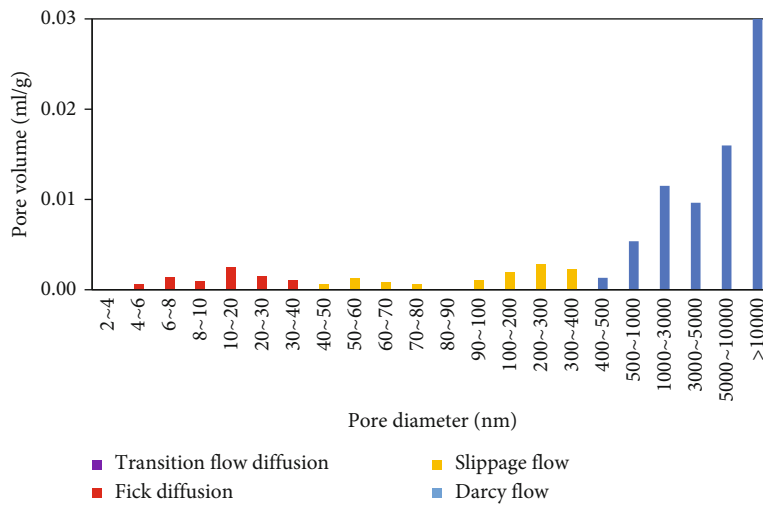
(c)

Figure 15: Gas migration form of different pores in Qigequan Formation mudstones. (a) H-3: pure mudstone, Fick diffusion, and slippage flow; (b) H-6: silty mudstone, Fick diffusion, slippage flow, and Darcy flow; (c) H-7: sandy mudstone and Darcy flow.
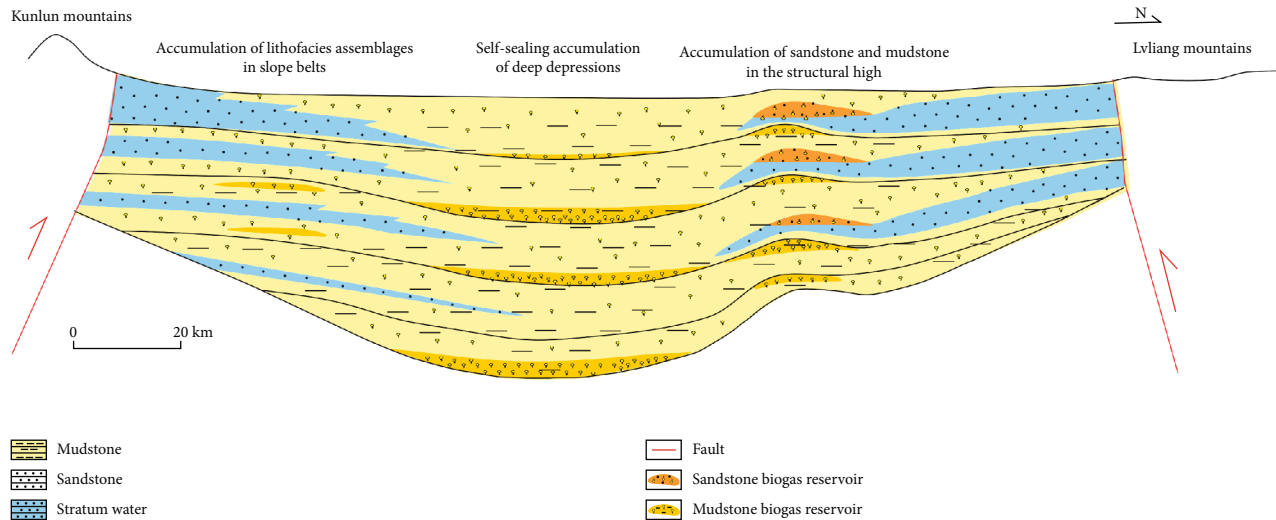
FIGURE 16: Model figure of biogas enrichment and accumulation in Qigequan Formation.

than 70%. Mudstone expands with clay minerals under high salinity and water content and has the characteristics of low permeability and high breakthrough pressure. Due to changes in lithology, methane gas in silty mudstone and sandy mudstone is blocked by water-bearing pure mudstone layers, lithofacies assemblages control the formation of biogas reservoirs. In the northern structural high of the Sandhu area, the porosity of mudstone becomes relatively larger. Mudstone cannot form a self-contained environment to store gas. However, the methane gas generated in the center of the depression migrated to the high strata by means of diffusion and sandstone seepage. The organic matter in the mudstone in the high position continuously generates hydrocarbons, and the sealing of hydrocarbon concentration plays a role in sealing the underlying strata. At the same time, methane is continuously supplied to the overlying sandstone. Therefore, the superimposed dynamic normal pressure gas reservoir of mudstone unconventional biogas reservoir and sandstone conventional biogas reservoir can be formed in the structural high position (Figure 16).

6. Conclusions

(1) The mudstone of the Qigequan Formation mainly develops rigid mineral intergranular pores, clay mineral pores, intragranular dissolved pores, and rare organic matter pores. The pore size distribution of different mudstones is complex, and the peak range of the pore size distribution curve is widely distributed. Pure mudstone and silty mudstone develop many nanopores, and the main pores developed range from 6 to 90 nm and 40 to 200 nm. However, the micron pores of sandy mudstone are mainly developed in the range of 0.5~10 μm. The mesopores of mudstone contribute 65.71%~93.49% of the total specific surface area and 3.74%~62.36% of the total pore volume, indicating that the ability of mesopores

to provide specific surface area is much larger than that of macropores, which is the prominent place for methane adsorption in mudstone reservoirs

(2) The contents of rigid and clay minerals in the mudstones of the Qigequan Formation have a perfect linear relationship with the pore structure parameters of the mesopores and macropores of the mudstone reservoirs. It shows that rigid minerals and clay minerals are the most important controlling factors for the micro-nanopore structure of mudstone. The increase in rigid mineral content is not conducive to the development of mesopores but favors the development of macropores or larger micron pores or microfractures. The rise of clay mineral content benefits mesopore development and provides essential specific surface area for gas adsorption

(3) The development characteristics of mudstone reservoirs in the Qigequan Formation create its unique gas accumulation form. The migration form of pure mudstone gas is mainly Fick diffusion and detachment flow, which has the characteristics of self-sealing accumulation. The migration form of silty mudstone gas is the coexistence of Fick diffusion, slippage flow, and Darcy flow, which has the characteristics of self-sealing and Darcy flow accumulation. The flow model of sandy mudstone gas is mainly Darcy flow, which only has the features of Darcy flow accumulation. Therefore, the difference in the development of reservoir pore structure creates different biogas accumulation models

Data Availability

Some of the data are contained in a published source cited in the references. All the data in this article is accessible to the readers.

Conflicts of Interest

The authors declare that they have no known competing financial interests or personal relationships that could have appeared to influence the work reported in this paper.

Authors' Contributions

H.S. (Shijie He) completed the original draft preparation; T.X. (Xianglu Tang) completed the review and editing; S.Z. (Zeyu Shao), J.Z. (Zhenxue Jiang), and W.B. (Bo Wang) completed project management and design; L.X. (Xiaoxue Liu) and W.Y. (Yuchao Wang) completed the data analysis and processing; and X.M. (Mingli Xu) completed the modification of the figures. All authors have read and agreed to the published version of the manuscript.

Acknowledgments

References

[1] S. Song, Y. Niu, L. Su, and X. Xia, "Tectonics of the north Qilian orogen, NW China," *Gondwana Research*, vol. 23, no. 4, pp. 1378–1401, 2013.

[2] J. Zhang, S. Yu, and C. G. Mattinson, "Early Paleozoic polyphase metamorphism in northern Tibet, China," *Gondwana Research*, vol. 41, pp. 267–289, 2017.

[3] Y. Shuai, S. Zhang, D. Ma et al., "Quaternary biogenic gases in the Qaidam Basin, Western China," *Bulletin of Canadian Petroleum Geology*, vol. 63, no. 1, pp. 75–83, 2015.

[4] Q. Chen, Z. Fan, S. Qin, F. Ma, and L. Wu, "Quaternary evaporites of biogenic methane gas in the eastern Qaidam Basin, China," *China. Carbonates and Evaporites*, vol. 31, no. 2, pp. 213–218, 2016.

[5] Y. Zong, L. Yong, Y. Wei, and T. Wang, "Research and application of production techniques for quaternary loose sand reservoirs in Sebei gas field," *Natural Gas Geoscience*, vol. 21, no. 3, pp. 357–361, 2010.

[6] L. Chen, Z. Jiang, K. Liu, and F. Gao, "Quantitative characterization of micropore structure for organic-rich lower Silurian shale in the upper Yangtze platform, South China: implications for shale gas adsorption capacity," *Advances in Geo-Energy Research*, vol. 1, no. 2, pp. 112–123, 2017.

[7] X. Yang and S. Guo, "Porosity model and pore evolution of transitional shales: an example from the Southern North China Basin," *Petroleum Science*, vol. 17, no. 6, pp. 1512–1526, 2020.

[8] F. Zhang, Z. Jiang, W. Sun et al., "Effect of microscopic pore-throat heterogeneity on gas-phase percolation capacity of tight sandstone reservoirs," *Energy & Fuels*, vol. 34, no. 10, pp. 12399–12416, 2020.

[9] K. Liu, M. Ostadhassan, Z. Jie, T. Gentzis, and R. Rezaee, "Nanoscale pore structure characterization of the Bakken shale in the USA," *Fuel*, vol. 209, pp. 567–578, 2017.

[10] J. Li, S. Lu, G. Chen, M. Wang, S. Tian, and Z. Guo, "A new method for measuring shale porosity with low-field nuclear

[11] F. Zhang, Z. Jiang, W. Sun et al., "A multiscale comprehensive study on pore structure of tight sandstone reservoir realized by nuclear magnetic resonance, high pressure mercury injection and constant-rate mercury injection penetration test," *Marine and Petroleum Geology*, vol. 109, pp. 208–222, 2019.

[12] D. Ross and R. M. Bustin, "The importance of shale composition and pore structure upon gas storage potential of shale gas reservoirs," *Marine & Petroleum Geology*, vol. 26, no. 6, pp. 916–927, 2009.

[13] R. G. Loucks, R. M. Reed, S. C. Ruppel, and U. Hammes, "Spectrum of pore types and networks in mudrocks and a descriptive classification for matrix-related mudrock pores," *AAPG Bulletin*, vol. 96, no. 6, pp. 1071–1098, 2012.

[14] H. Li, H. Tang, and M. Zheng, "Micropore structural heterogeneity of siliceous shale reservoir of the Longmaxi formation in the southern Sichuan Basin, China," *Minerals*, vol. 9, no. 9, pp. 548–568, 2019.

[15] N. Peng, S. He, Q. Hu et al., "Organic nanopore structure and fractal characteristics of Wufeng and lower member of Longmaxi shales in southeastern Sichuan, China," *Marine and Petroleum Geology*, vol. 103, pp. 456–472, 2019.

[16] H. Xu, W. Zhou, R. Zhang, S. Liu, and Q. Zhou, "Characterizations of pore, mineral and petrographic properties of marine shale using multiple techniques and their implications on gas storage capability for Sichuan Longmaxi gas shale field in China," *Fuel*, vol. 241, pp. 360–371, 2019.

[17] M. Sun, B. Yu, Q. Hu et al., "Pore characteristics of Longmaxi shale gas reservoir in the northwest of Guizhou, China: investigations using small-angle neutron scattering (SANS), helium pycnometry, and gas sorption isotherm," *International Journal of Coal Geology*, vol. 171, pp. 61–68, 2017.

[18] R. Yang, S. He, Q. Hu, M. Sun, D. Hu, and J. Yi, "Applying SANS technique to characterize nano-scale pore structure of Longmaxi shale, Sichuan Basin (China)," *Fuel*, vol. 197, no. 1, pp. 91–99, 2017.

[19] Y. Liang, J. Zhang, Y. Liu et al., "Evidence for biogenic silica occurrence in the lower Silurian Longmaxi shale in southeastern Chongqing, China," *Minerals*, vol. 10, no. 11, pp. 945–967, 2020.

[20] Q. Gou, S. Xu, F. Hao, F. Yang, Z. Shu, and R. Liu, "The effect of tectonic deformation and preservation condition on the shale pore structure using adsorption-based textural quantification and 3D image observation," *Energy*, vol. 219, pp. 119579–119598, 2021.

[21] C. R. Clarkson, N. Solano, R. M. Bustin et al., "Pore structure characterization of north American shale gas reservoirs using USANS/SANS, gas adsorption, and mercury intrusion," *Fuel*, vol. 103, pp. 606–616, 2013.

[22] S. Jiang, Z. Xu, Y. Feng et al., "Geologic characteristics of hydrocarbon-bearing marine, transitional and lacustrine shales in China," *Journal of Asian Earth Sciences*, vol. 115, pp. 404–418, 2016.

[23] S. Guo and C. Chen, "Sequence stratigraphy of Quaternary Seven Spring Group of Sanhu Depression and prediction of favorable targets," *Earth Science Frontiers*, vol. 15, no. 2, pp. 43–50, 2008.

[24] S. Zhang, M. Li, Y. Shuai, L. Huang, A. Su, and Z. Li, "Biogeochemical identification of the Quaternary biogenic gas source

rock in the Sanhu Depression, Qaidam Basin," *Organic geochemistry*, vol. 73, pp. 101–108, 2014.

[25] S. Chen, Y. Zhang, L. Wu et al., "Cenozoic structural deformation in the Yuqia-Jiulongshan region, northern Qaidam Basin, China," *Petroleum Exploration and Development*, vol. 47, no. 1, pp. 114–123, 2020.

[26] X. Gu, D. Cole, G. Rother, D. F. R. Mildner, and S. L. Brantley, "Pores in Marcellus shale: a neutron scattering and FIB-SEM study," *Energy & Fuels*, vol. 29, no. 3, pp. 1295–1308, 2015.

[27] F. Li, M. Wang, S. Liu, and Y. Hao, "Pore characteristics and influencing factors of different types of shales," *Marine and Petroleum Geology*, vol. 102, pp. 391–401, 2019.

[28] J. Zhang, X. Li, G. Zhang, X. Zou, F. Wang, and Y. Tang, "Microstructural investigation of different nanopore types in marine- continental transitional shales: examples from the Longtan formation in Southern Sichuan Basin, south China," *Marine and Petroleum Geology*, vol. 110, pp. 912–927, 2019.

[29] X. Wang, B. Zhang, Z. He et al., "Electrical properties of Longmaxi organic-rich shale and its potential applications to shale gas exploration and exploitation," *Journal of Natural Gas Science & Engineering*, vol. 36, pp. 573–585, 2016.

[30] Q. Huang, Q. Dou, and Y. Sun, "Characterization of pore structure variation and permeability heterogeneity in carbonate rocks using MICP and sonic logs: Puguang gas field, China," *Petropysics*, vol. 58, no. 6, pp. 576–591, 2017.

[31] Z. L. Huang, X. B. Guo, and B. Liu, "The reservoir space characteristics and origins of Lucaogou formation source rock oil in the Malang sag," *Acta Sedimentologica Sinica*, vol. 30, no. 6, pp. 1115–1122, 2012.

[32] H. Wang, L. Chen, Z. Qu et al., "Modeling of multi-scale transport phenomena in shale gas production – a critical review," *Applied Energy*, vol. 262, pp. 114575–114608, 2020.

[33] H. Zhu, T. Zhang, X. Liang, Z. Zhang, and L. Zhang, "Insight into the pore structure of Wufeng-Longmaxi black shales in the South Sichuan Basin, China," *Journal of Petroleum Science and Engineering*, vol. 171, pp. 1279–1291, 2018.

[34] S. Brunauer, P. H. Emmett, and E. Teller, "Adsorption of gases in multimolecular layers," *Journal of the American Chemical Society*, vol. 60, no. 2, pp. 309–319, 1938.

[35] E. Barrett, L. Joyner, and P. Halenda, "The determination of pore volume and area distributions in porous substances. I. Computations from nitrogen isotherms," *Journal of the American Chemical society*, vol. 73, no. 1, pp. 373–380, 1951.

[36] Z. Li, I. A. Oyediran, R. Huang et al., "Study on pore structure characteristics of marine and continental shale in China," *Journal of Natural Gas Science and Engineering*, vol. 33, pp. 143–152, 2016.

[37] Y. Wang, L. Liu, S. Zheng, Z. Luo, Y. Sheng, and X. Wang, "Full-scale pore structure and its controlling factors of the Wufeng-Longmaxi shale, southern Sichuan Basin, China: implications for pore evolution of highly overmature marine shale," *Journal of Natural Gas Science and Engineering*, vol. 67, pp. 134–146, 2019.

[38] B. Liu, J. Teng, M. Mastalerz, J. Schieber, A. Schimmelmann, and D. Bish, "Compositional control on shale pore structure characteristics across a maturation gradient: insights from the Devonian New Albany shale and Marcellus shale in the eastern United States," *Energy and Fuels*, vol. 35, no. 9, pp. 7913–7929, 2021.

[39] Z. Gao, Y. Fan, Q. Xuan, and G. Zheng, "A review of shale pore structure evolution characteristics with increasing thermal maturities," *Advances in Geo-Energy Research*, vol. 4, no. 3, pp. 247–259, 2020.

[40] J. Xu, Q. Jin, X. Xu et al., "Factors controlling organic-rich shale development in the Liushagang Formation, Weixinan Sag, Beibu Gulf Basin: implications of structural activity and the depositional environment," *Petroleum Science*, vol. 18, no. 4, pp. 1011–1020, 2021.

[41] X. Ma and S. Guo, "Comparative study on shale characteristics of different sedimentary microfacies of late Permian Longtan formation in southwestern Guizhou, China," *Minerals*, vol. 9, no. 1, pp. 20–52, 2018.

[42] W. Ji, Y. Song, Z. Jiang et al., "Fractal characteristics of nanopores in the lower Silurian Longmaxi shales from the upper Yangtze platform, South China," *Marine and Petroleum Geology*, vol. 78, pp. 88–98, 2016.

[43] F. Yang, Z. Ning, Q. Wang, R. Zhang, and B. M. Krooss, "Pore structure characteristics of lower Silurian shales in the southern Sichuan Basin, China: insights to pore development and gas storage mechanism," *International Journal of Coal Geology*, vol. 156, pp. 12–24, 2016.

[44] Y. Ma, N. Zhong, L. Cheng et al., "Pore structure of the graptolite-derived OM in the Longmaxi Shale, southeastern upper Yangtze region, China," *Marine & Petroleum Geology*, vol. 72, pp. 1–11, 2016.

[45] Y. He, J. Cheng, X. Dou, and X. Wang, "Research on shale gas transportation and apparent permeability in nanopores," *Journal of Natural Gas Science & Engineering*, vol. 38, pp. 450–457, 2017.

[46] B. Zhang, X. Li, Y. Zhao, C. Chang, and J. Zheng, "A review of gas flow and its mathematical models in shale gas reservoirs," *Geofluids*, vol. 2020, Article ID 8877777, 19 pages, 2020.

[47] D. Moghad and M. Jamiolahmady, "Slip flow in porous media," *Fuel*, vol. 173, pp. 298–310, 2016.

[48] L. Chen, Q. Kang, R. Pawar, Y. L. He, and W. Q. Tao, "Pore-scale prediction of transport properties in reconstructed nanostructures of organic matter in shales," *Fuel*, vol. 158, no. 15, pp. 650–658, 2015.

[49] F. Sun, Y. Yao, G. Li, and X. Li, "A slip-flow model for multi-component shale gas transport in organic nanopores," *Arabian Journal of Geosciences*, vol. 12, no. 5, pp. 143–154, 2019.

[50] X. Wang, L. Liu, Y. Wang et al., "Comparison of the pore structures of lower Silurian Longmaxi formation shales with different lithofacies in the southern Sichuan Basin, China," *Journal of Natural Gas Science and Engineering*, vol. 81, pp. 103419–103431, 2020.

[51] W. Lin, "A slip model for rarefied gas flows at arbitrary Knudsen number," *Applied Physics Letters*, vol. 93, no. 25, pp. 94–98, 2008.

[52] C. Kim, H. Jang, and J. Lee, "Experimental investigation on the characteristics of gas diffusion in shale gas reservoir using porosity and permeability of nanopore scale," *Journal of Petroleum Science & Engineering*, vol. 133, pp. 226–237, 2015.

[53] K. Wu, Z. Chen, X. Li et al., "Flow behavior of gas confined in nanoporous shale at high pressure: real gas effect," *Fuel*, vol. 205, pp. 173–183, 2017.

[54] W. Yuan, Z. Pan, L. Xiao et al., "Experimental study and modelling of methane adsorption and diffusion in shale," *Fuel*, vol. 117, pp. 509–519, 2014.